FISEVIER

Contents lists available at ScienceDirect

Lithos

journal homepage: www.elsevier.com/locate/lithos



Research Article

Petrogenesis of gold-bearing listvenites from the carbonatized mantle section of the Neoproterozoic Ess ophiolite, Western Arabian Shield, Saudi Arabia



Hisham A. Gahlan a,b,*, Mokhles K. Azer c, Paul D. Asimow d, Khaled M. Al-Kahtany e

- ^a Department of Geology and Geophysics, King Saud University, Riyadh 11451, Saudi Arabia
- ^b Geology Department, Assiut University, Assiut 71516, Egypt
- ^c Geological Sciences Department, National Research Centre, Cairo, Egypt
- d Division of Geological & Planetary Sciences, California Institute of Technology, Pasadena, CA 91125, USA
- ^e Seismic Studies Center, College of Science, King Saud University, Riyadh 11451, Saudi Arabia

ARTICLE INFO

Article history: Received 12 June 2020 Received in revised form 2 July 2020 Accepted 3 July 2020 Available online 12 July 2020

Keywords: Arabian Shield Ophiolite Listvenite Fuchsite Sulphides Gold

ABSTRACT

The variably serpentinized mantle peridotites of the Late Neoproterozoic Ess ophiolite (Western Saudi Arabia) are highly altered along shear zones and thrust planes to form erosion-resistant listvenites. The listvenites are distinguished petrographically and geochemically into three types: carbonate, silica-carbonate and silica (birbirite) listvenites. Geochemical analyses are consistent with expectations from petrography: carbonate listvenite is low in SiO₂ content but high in MgO, Fe₂O₃, and CaO relative to silica-carbonate and birbirite, which is remarkably high in SiO₂ at the expense of all other components. The total REE contents are low in silica-carbonate and carbonate listvenites but highly enriched in birbirite, with a large positive Eu anomaly. The host serpentinites have all the characteristics typically associated with highly depleted mantle harzburgite protoliths in supra-subduction fore-arc settings: bulk compositions are low in Al₂O₃ and CaO with high Mg# [molar Mg/(Mg + Fe)], relict Cr-spinel has high Cr# [molar Cr/(Cr + Al)] and low TiO_2 , and relict olivine has high Mg# and NiO content. The Cr-spinel relics are also found in the listvenites; those in serpentinite and carbonate listvenites have significantly higher Mg# than those in silica-carbonate and birbirite, suggesting reequilibration of Cr-spinel in the later phases of listvenitization. The varieties of listvenite capture successive stages of fluid-mediated replacement reactions. The carbonate listvenite appears to have developed syncontemporaneously with serpentinization, whereas silica-carbonate listvenite and birbirite formed later. The listvenite formation resulted in leaching and removal of some components accompanied by deposition of others in the solid products, notably CO₃, SiO₂, REE (especially Eu), Au, Zn, As, Sb and K. Our data show that listvenitization concentrated gold at sub-economic to economic grades; measured gold concentrations in the host serpentinite are 0.5-1.7 ng/g, versus 4-2569 ng/g in carbonate listvenite, 43-3117 ng/g in silicacarbonate listvenite and 5-281 ng/g in birbirite. The listvenite deposits in the Jabal Ess area merit further exploration for gold.

© 2020 Elsevier B.V. All rights reserved.

1. Introduction

Ophiolite sequences are an important lithologic component of the Neoproterozoic Arabian Shield, the eastern part of the Arabian-Nubian Shield (ANS). The ANS is a juvenile tract of continental crust that forms the northern part of the East African Orogen (e.g. Johnson and Woldehaimanot, 2003; Stoeser and Frost, 2006). It formed in Neoproterozoic time from a collage of Neoproterozoic juvenile arcs,

E-mail address: hjhlan@yahoo.com (H.A. Gahlan).

younger volcano-sedimentary successions and voluminous granitoid intrusions with enclaves of pre-Neoproterozoic crust (e.g., Ali et al., 2010; Johnson and Woldehaimanot, 2003; Stoeser and Frost, 2006).

The ophiolitic rocks of the Arabian Shield are fragments of upper mantle and oceanic crust that were obducted, tectonically emplaced over continental crust, and preserved above sea level. Most Arabian Shield ophiolites have been dismembered through multiple phases of alteration, deformation and metamorphism (e.g., Abuamarah et al., 2020; Gahlan et al., 2020a; Gahlan et al., 2020b; Johnson et al., 2004; Stern et al., 2004). Their ultramafic mantle sections have been conspicuously altered by circulation and infiltration of various hydrothermal fluids at various temperatures, leading to assemblages including

 $^{^{\}ast}$ Corresponding author at: Department of Geology and Geophysics, King Saud University, Riyadh 11451, Saudi Arabia.

serpentinite, listvenite and talc-carbonate rocks. Mobilization of elements in these fluids makes the alteration products valuable targets for mineral exploration.

In recent decades, the silica-carbonate alteration (listvenitization) of ophiolitic rocks has been a matter of particular interest because of its spatial and temporal association with gold mineralization (e.g. Buisson and Leblanc, 1987; Hansen et al., 2005; Pirouei et al., 2020; Uçurum, 2000; Uçurum and Larson, 1999). However, the genetic relationship between Au enrichment and listvenite formation remains unclear. The understanding of listvenite formation and the associated mineralization enables refinement of existing petrogenetic models and exploration strategies and may also have implications for mitigation of anthropogenic CO₂ emissions (e.g. Beinlich et al., 2012; van Noort et al., 2013). Numerous listvenites are mentioned in the Arabian Shield geological literature (e.g., Al Jahdali, 2004; Al Jahdali et al., 2003; Al Shanti, 2009; Gahlan et al., 2020a; Gahlan et al., 2020b; Harbi et al., 2003, 2006), but no detailed studies of listvenites in Saudi Arabia are available.

The present work presents the first detailed study of listvenite associated with the late Neoproterozoic Ess ophiolite, including assessment of their potential as a source of gold. We present field observations, petrographic description, mineral chemistry and bulk-rock geochemical data. These data allow us to constrain the timing, compositions and sources of the fluids involved in the listvenitization. We propose a basic conceptual model of listvenitization in the area, intended as an exploration tool for potential economic-grade mineralization in Saudi Arabia.

2. General geology and field observations

Neoproterozoic exposures in Saudi Arabia are part of the Arabian Shield, which was a contiguous part of the ANS before the opening of the Red Sea. The Arabian Shield occupies much of western Saudi Arabia and has smaller exposures in southern Levant, southern Jordan, and in Yemen. Ophiolite sequences within the Arabian Shield are fragments of oceanic lithosphere that were obducted onto continental crust during the collision between West and East Gondwana upon closure of the Mozambique Ocean (e.g. Gahlan et al., 2020a; Gahlan et al., 2020b; Pallister et al., 1988; Stern et al., 2004). Most Arabian Shield ophiolites are incomplete, lacking one or more of the typical lithologies of an ophiolite sequence, as a result of dismemberment, folding, shearing, or limited exposure. The Ess ophiolite, however, although somewhat disrupted and deformed, is a complete classical ophiolite, including a lower "mantle" unit of serpentinized peridotite and an upper "crustal" unit of layered and isotropic gabbro, sheeted dykes, pillow basalts and pelagic sediments.

Listvenite has been reported in many areas of the Arabian Shield (Al Jahdali, 2004; Al Jahdali et al., 2003; Al Shanti, 2009; Harbi et al., 2003, 2006). Al Shanti (2009) ascribed the widespread transformation of serpentinites to silicic carbonate (listvenite) along sheared sutures to post-tectonic deformation and hydrothermal solution activity. Harbi et al. (2006), Al Jahdali et al. (2003) and Al Jahdali (2004) studied listvenite associated with serpentinites at Jabal Ghadarah. These authors noted significant gold enrichment, particularly along the N-S trending Nabitah ophiolite belt.

The Jabal Ess area is situated in the northwestern corner of Saudi Arabia, about 400 km NW of Al Madinah Al Munawarah city (Fig. 1). Geotectonically, the area lies near the NE end of the Yanbu Suture at the join between the Midyan and Hijaz terranes. The Ess ophiolite, exposing at least 3 km of section, is the most complete and the best-preserved ophiolitic section in the Arabian shield (Al-Shanti, 1982; Johnson et al., 2004; Al Shanti, 2009). Detailed field work in the Ess area is reported in Gahlan et al. (2020a).

In addition to the ophiolitic sequence itself, rock units exposed in the Jabal Ess area include metavolcanic and metasedimentary rocks, intrusive granitoid rocks, and Phanerozoic sedimentsary units (Fig. 2). Like most Arabian Shield ophiolites, the Ess ophiolite occurs as folded

allochthonous thrust sheets within metasedimentary and metavolcanic host rocks. The Ess ophiolite contains all the components of a complete ophiolite succession, but some parts are faulted and appear out-of-sequence; it is variably deformed, metamorphosed, and cross-cut by abundant vertical faults marked by significant brecciation. The lower unit of serpentinized mantle rocks is overlain by an ultramafic cumulate sequence, layered and isotropic gabbros, sheeted dykes, pillow lavas and pelagic sediments (Gahlan et al., 2020a). The mantle section is composed mainly of serpentinized harzburgite and dunite with pods of chromitite and pyroxenite. Deformation and schistosity are common in the serpentinites and some highly sheared samples are brecciated. Extensive metasomatism and alteration has transformed the ultramafic rocks to talc-carbonates, magnesite deposits and listvenites, especially along shear zones and fault planes.

Listvenite bodies of various shapes and sizes are observed along shear zones cutting the mantle section. In the field, the listvenites are easy to distinguish from other associated rocks; they reliably form upstanding erosion-resistant ridges. The shear zones or thrust faults marked by listvenite strike NNE-SSW or NE-SW, dip to the NW, and typically feature discontinuous sheet-like bodies of listvenite in their hanging walls and serpentinite in their footwalls.

The listvenites of Jabal Ess are distinguished in the field into carbonate listvenite, silica-carbonate listvenite and silica listvenite (birbirite). The carbonate listvenite is the most common type; it is characterized by yellowish-brown to reddish-brown color due to iron oxide stain, presumably reflecting oxidative weathering of Fe-bearing carbonates (Fig. 3a). A few dolomite-quartz veins and irregular pockets of quartz are observed in the carbonate listvenite (Fig. 3b). The boundaries of carbonate listvenites are progressive, distributed transition zones of partly listvenitized serpentinite (Fig. 3c), ~0.3–0.5 m wide and grey to greenish-grey in color. Veinlets of carbonates can be traced throughout these zones. Deformation and schistosity similar to that in serpentinite is seen in many outcrops of carbonate listvenite.

The silica-carbonate listvenite is grey- to buff-colored, with bright green flecks of fuchsite (Fig. 3d). This type of listvenite characteristically shows rhythmic banding of quartz and carbonate minerals (Fig. 3e). Small fragments of unaltered serpentinite can be found within silica-carbonate listvenite. In a few outcrops, sparse gossan-like alteration areas cover the silica-carbonate listvenite.

At the top of the Jabal Ess, the listvenites are capped by silica listvenite (birbirite), a hard and erosion-resistant siliceous rock. It forms sheets or veins cutting carbonate- and silica-carbonate listvenite. Some Fe-rich birbirite samples are characterized by deep red to brown color. Other outcrops of birbirite are brecciated or mylonitized along later faults. The formation of birbirite at the expense of other listvenites is suggested by included listvenite fragments of various sizes (Fig. 3f).

3. Analytical methods

Representative samples of listvenites and the associated serpentinite were selected for the preparation of polished thin sections. Detailed petrographic study included both polarizing transmitted and reflected light microscopy.

X-ray powder diffraction (XRD) analysis was used to determine the mineralogical composition of selected listvenite samples. A Bruker D8 advanced X-ray diffractometer at the Central Metallurgical and Development Institute in Cairo, Egypt, was operated with Cu radiation at 40 kV and 40 mA and a secondary monochrometer. The scanning speed was 1°/min in a conventional 2θ scan. Mineral identification based on American Standard Test Materials (ASTM) cards considered both *d*-values and relative intensities of observed diffraction peaks.

Polished sections of selected samples of listvenite were examined with a Philips XL30 environmental scanning electron microscope (ESEM) at the Nuclear Materials Authority in Egypt. The SEM was operated at 25 kV and equipped with an EDAX energy dispersive X-ray spectrometer (EDS) able to detect elements with atomic number greater

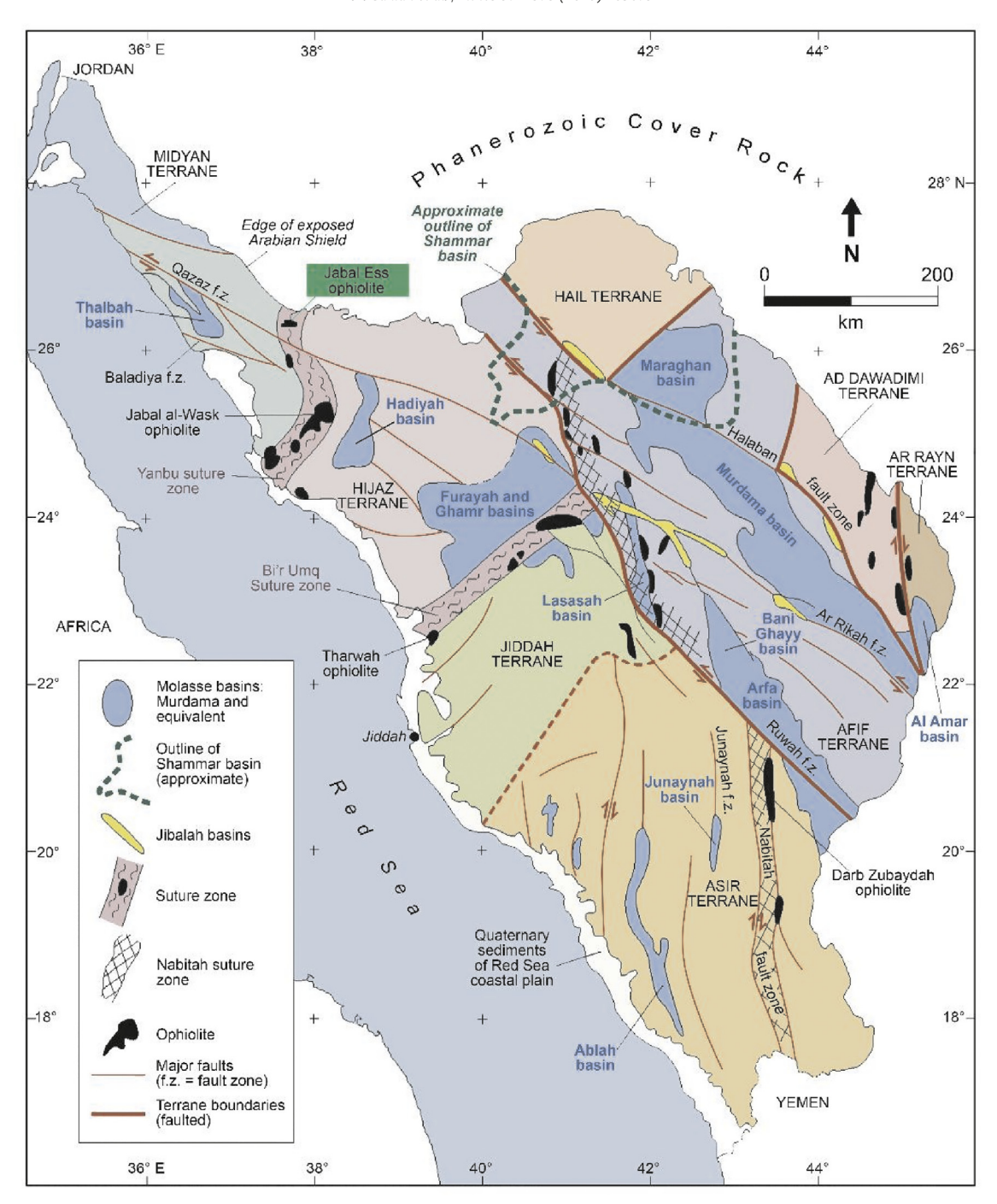


Fig. 1. Regional tectonic map of the Arabian Shield showing ophiolite belts along suture zones, major faults, terranes and sedimentary basins in western Saudi Arabia (after Nehlig et al., 2002).

than 4 (e.g., B); counting rates were maintained in the 1000–1500 counts per second range.

Mineral chemical analyses were obtained with a CAMECA SX100 electron probe at the Department of Geosciences, University of Oslo, Norway. Polished thin sections were carbon-coated and analyzed with a 15 kV, 15 nA, 2 µm diameter beam for 10 s counting time on-peak and 5 s each at low and high background positions. A ZAF matrix correction routine was used. Calculations of the mineral structural formulae used appropriate software including custom spreadsheets.

Representative samples of listvenites (26 samples) and serpentinite (7 samples) were analyzed for major, trace and rare earth elements at Activation Laboratories Ltd. (Actlabs, Canada). The samples for chemical

analyses were crushed in an agate mortar, quartered several times to obtain representative samples, and powdered to ~40 mesh in an agate ring mill. The major oxides were measured by lithium metaborate/ tetraborate fusion ICP-AES. Trace and rare earth elements were measured by ICP-MS following lithium borate fusion and acid digestion. In addition, a separate 0.5 g split was digested in hot (95 °C) Aqua Regia and analyzed by ICP-MS to determine precious and base metals. The detection limits for the major oxides are between 0.01% and 0.04%, while those for trace and rare earth elements are 0.01 and 0.5 and 0.01–0.1 μ g/g, respectively. All trace and REE elements concentration are given in micrograms per gram (μ g/g) except gold, which is given in nanograms per gram (η g/g). Loss on ignition (LOI) was determined

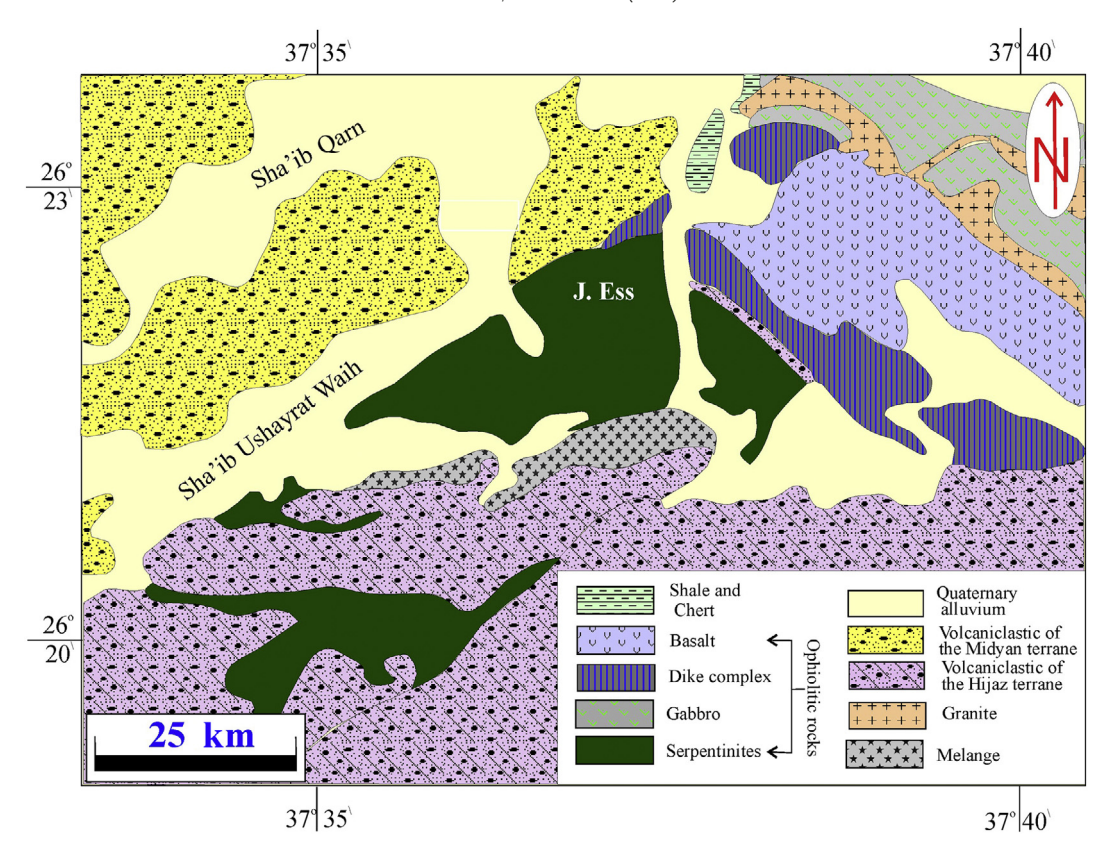


Fig. 2. Geologic map of the Jabal Ess area (modified after Johnson et al., 2004).

by weight difference after ignition at 1000 °C. Precision and accuracy were controlled by analysis of international reference materials and replicate analyses and are 1% for major elements and 2% to 5% for trace elements. Details of analytical precision, standardization, and detection limits are given on the Actlabs website (actlabs.com).

4. Petrography

This section summarizes transmitted and reflected light petrographic results for host serpentinite and each type of listvenite. Mineral identifications given in this section have been verified where necessary by XRD, microprobe and ESEM analysis.

4.1. Serpentinite

The mantle section of the Ess ophiolite is uniformly fully serpentinized but expresses a range of deformation textures from massive to highly sheared. All the studied sections are dominated by serpentine minerals alongside carbonates, amphiboles and opaques. Massive serpentinites preserve sparse fresh relics of primary olivine, pyroxene and Cr-spinel. XRD analyses show that the serpentine is mainly antigorite with minor amounts of chrysotile and lizardite. The sheared serpentinite is mineralogically similar to massive serpentinite except that relics of primary minerals are generally absent; the schistosity apparent in hand-sample is expressed at microscopic scale by subparallel alignment of serpentine flakes (Fig. 4a).

Although the primary minerals and textures of the ultramafic rocks are almost completely replaced by serpentine, the abundance of mesh texture (after olivine) and bastite texture (after orthopyroxene) suggests harzburgite protoliths. Where fresh relics of primary olivine are preserved, they form small to medium-grained rounded crystals, cracked and dissected by networks of serpentine veins in interlocking

textures (Fig. 4b). Scarce fresh relics of orthopyroxene are present in bastite-textured areas (Fig. 4c). Very rare fresh relics of clinopyroxene can be found as well. Some samples of serpentinite, especially the sheared variety, are rich in carbonate minerals (~10–25 vol%), mainly magnesite with rare calcite and dolomite. Carbonates occur as cryptocrystalline sparse crystals and fine aggregates, stained reddish-brown by finely disseminated iron oxide inclusions. Sheared samples also contain sparse fibrous crystals and lamellae of tremolite–actinolite (Fig. 4d).

Cr-spinel, magnetite and sulfides are the main opaque minerals. Cr-spinel occurs as deep reddish-brown, subhedral to euhedral, disseminated crystals and as irregular grains. Along grain boundaries and cracks, Cr-spinel is partly replaced by inner rims of ferritchromite and outer rims of Cr-bearing magnetite (Fig. 4e, f). Very few sulfide grains are present; they include pyrite, arsenopyrite and chalcopyrite. Pyrite occurs mainly as euhedral to subhedral grains randomly scattered among the serpentine minerals. Chalcopyrite occurs as homogenous subhedral to anhedral crystals andand as intergrowths with pyrite.

4.2. Listvenites

The listvenites of Jabal Ess are fine- to medium-grained rocks. Colors in hand-sample may be light grey, brown-black, yellowish-brown or reddish-brown. Some listvenite samples are porous, and some are sheared to form a semi-schistose texture. Petrographic and XRD-based modal proportions of quartz and carbonate support the field-based division of the listvenites around Jabal Ess into three categories: carbonate listvenite, silica-carbonate listvenite and silica listvenite (birbirite).

4.2.1. Carbonate listvenite

The carbonate listvenite is composed of ≥60 vol% modal carbonate minerals, with the balance being mostly silica with minor opaque minerals. Scarce relics and accessory minerals include serpentine,

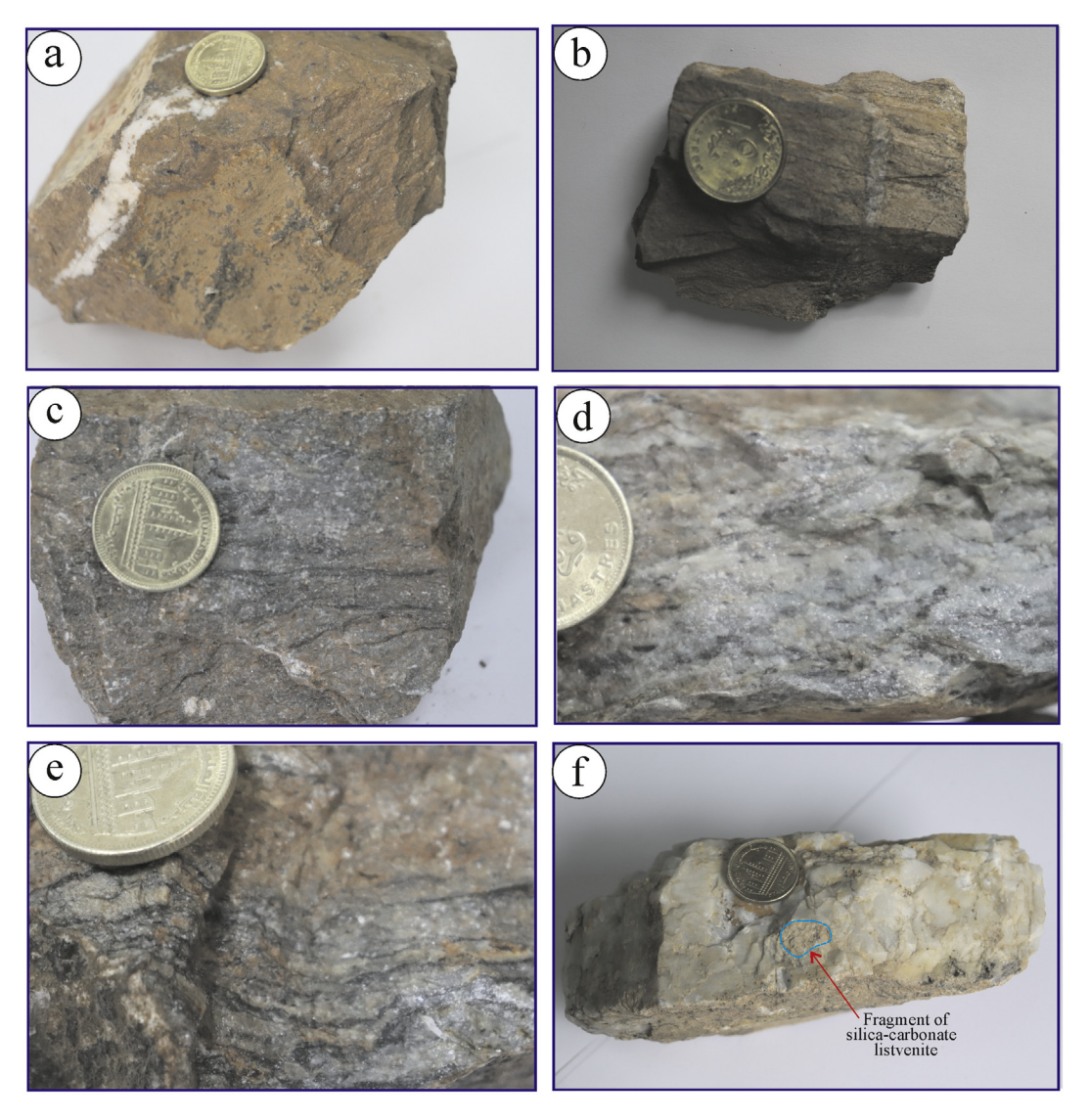


Fig. 3. Photographs of listvenite hand specimens from the Jabal Ess ophiolite: (a) reddish brown carbonate listvenite with irregular pockets of quartz; (b) quartz vein cutting carbonate listvenite; (c) transitional zone of listvenitized serpentinite; (d) silica-carbonate listvenite displaying greyish green to buff color with bright green fuchsite; (e) rhythmic banding of quartz and carbonate minerals in silica-carbonate listvenite; and (f) birbirite containing a small fragment of silica-carbonate listvenite. (For interpretation of the references to color in this figure legend, the reader is referred to the web version of this article.)

magnetite, chlorite, talc and rutile. XRD analyses indicate that magnesite is the dominant carbonate mineral, but both dolomite and calcite are also present in minor amounts. Magnesite occurs as euhedral to anhedral, fine- to coarse-grained crystals and as fine aggregates (Fig. 5a). Euhedral crystals of magnesite with well-formed cleavage indicate *in situ* crystallization. Some magnesite crystals are stained black by manganese oxide inclusions and some are similarly stained red by iron oxide. Dolomite occurs as late, coarse-grained veins that crosscut the fine-grained magnesite (Fig. 5b). Quartz occurs as microcrystalline to fine subhedral crystals and as small veinlets in the carbonate.

Opaque minerals in the carbonate listvenite are mainly Cr-spinel, sulfides and gold. Cr-spinel occurs as subhedral to anhedral cracked crystals (Fig. 5c), partly replaced by rims of ferritchromite. Sulfides include pyrite, pyrrhotite, arsenopyrite, sphalerite, chalcopyrite, galena, and pentlandite. Pyrite is the most common di-sulfide (s.l.) mineral, forming small anhedral to euhedral grains (Fig. 5d). Pyrite may contain inclusions of galena. Colloform goethite after pyrite is observed in many samples of carbonate listvenite. Pyrrhotite is a minor phase, as small, disseminated, anhedral crystals or rounded blebs enclosed in pyrite. Arsenopyrite occurs as subhedral to euhedral rhombic crystals, either

isolated or associated with pyrite. Minor sphalerite is found as small, disseminated, anhedral crystals or as small cross-cutting veinlets and fracture fillings. Sphalerite contains very small included blebs of chalcopyrite. Chalcopyrite also forms anhedral crystals, altered in places to covellite. Pentlandite is found mainly as small, randomly-scattered, anhedral to rounded grains (Fig. 5e). Scarce gold occurs as very fine specks along fractures (Fig. 5f).

4.2.2. Silica-carbonate listvenite

The silica-carbonate listvenite has more modal quartz and less carbonate than carbonate-listvenite. It consists mainly of quartz and carbonates with minor opaques, serpentine, chlorite, talc, and Cr-rich muscovite (fuchsite). This type of listvenite is characterized by the presence of fuchsite and by rhythmic banding of quartz and carbonate minerals (Fig. 6a); the bands are composed mainly of fine-grained to amorphous silica alternating with fine-grained carbonates. Rare quartz and magnesite veinlets cross-cut the banding. Coarse-grained magnesite, fine-grained magnesite, and magnesite veins can be recognized as three distinct generations of carbonate mineral growth. The first-generation coarse magnesite is often

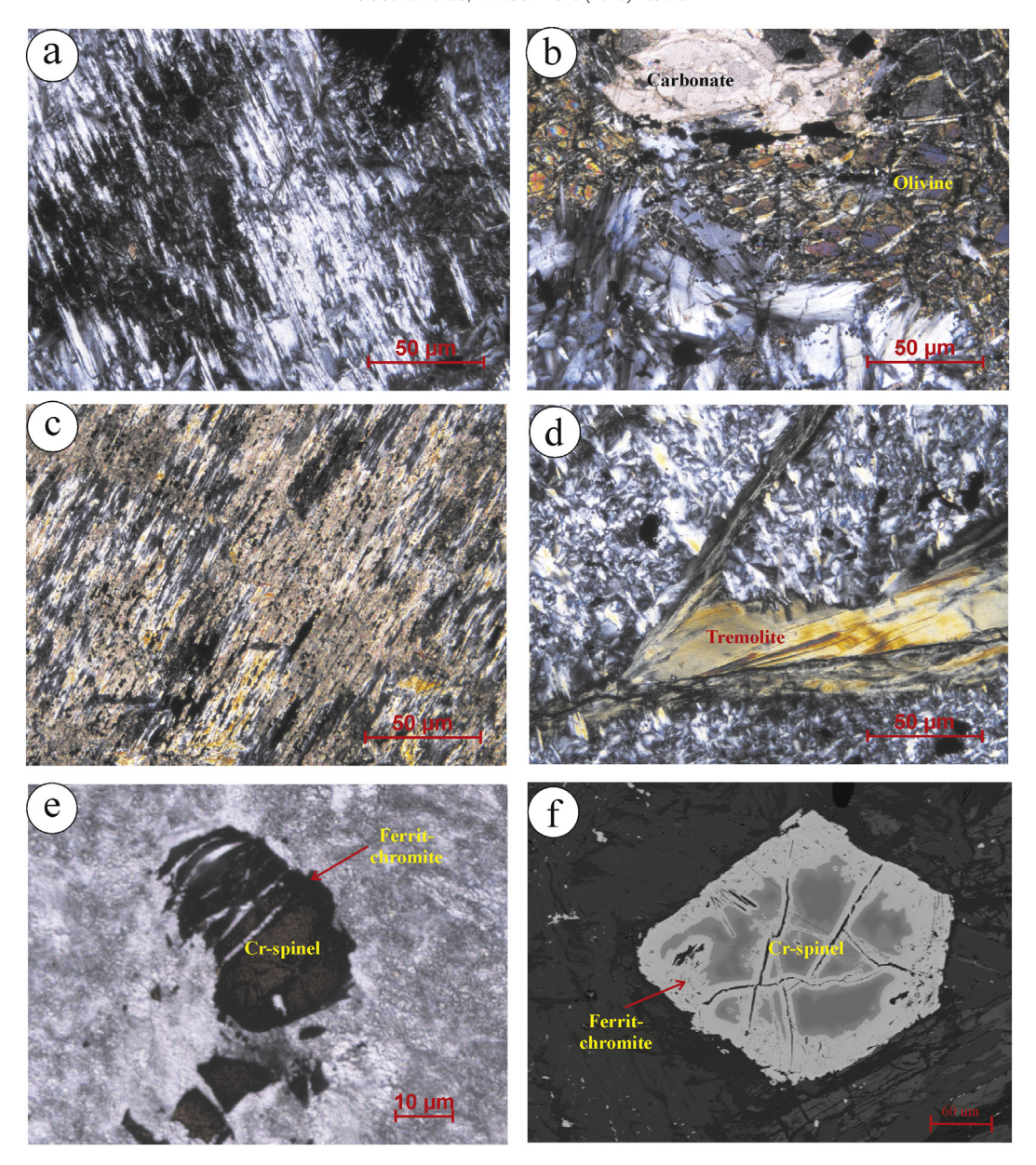


Fig. 4. Photomicrographs showing petrographic textures in serpentinite between crossed nicols (a, b, c and d), reflected light (e), and scanning electron microscope (SEM) backscatter (f): (a) schistosity in sheared serpentinite; (b) fresh relics of primary olivine forming interlocking textures; (c) fresh relics of orthopyroxene within bastite-textured serpentine; (d) fibers of tremolite in serpentine matrix; (e) deep reddish brown anhedral crystal of Cr-spinel altered along margins into dark ferritchromite; and (f) Cr-spinel showing fresh a core (dark grey backscatter) with rims of ferritchromite (higher backscatter). (For interpretation of the references to color in this figure legend, the reader is referred to the web version of this article.)

stained with iron oxides and variably deformed. Minor deformation is indicated by kink banding, whereas major deformation led to fragmentation and recrystallization to form the second-generation fine-grained aggregates. The cross-cutting veins represent the last phase of carbonate mineralization.

Quartz is found in silicate-carbonate listvenite as fine aggregates, fine- to coarse-grained subhedral crystals, and coarse-grained vein fillings. Talc is found as large plates and fine aggregates associated with antigorite bundles (Fig. 6b). Fuchsite, which notably requires the presence of potassium, occurs as fine green flakes, inclusions in carbonates, thin bands, surface veneers, and cavity fillings (Fig. 6c).

Reflected-light microscopy was used to distinguish opaque minerals including Cr-spinel, sulfides, and scarce native gold. Cr-spinel forms subhedral cracked crystals with dark grey color (Fig. 6d), altered to ferritchromite along grain boundaries and fractures. The silicacarbonate listvenite is richer in sulfide minerals than the other types,

and includes pyrite, pyrrhotite, sphalerite, arsenopyrite, and rare chalcopyrite. Pyrite occurs as randomly scattered euhedral to subhedral cubes and as fine specks partly or completely converted to goethite. Pyrrhotite occurs as anhedral specks along fractures. Randomly scattered, minute, anhedral to rounded, grains of pentlandite are occasionally found. Sphalerite occurs as fine disseminated crystals. Arsenopyrite forms small aggregates and intergrowths with pyrite. Chalcopyrite occurs as tiny disseminated crystals and as small inclusions in pyrite. Two phases of gold are observed in the silica-carbonate listvenite: as fine specks and blebs along fractures in quartz (Fig. 6e) and as inclusions within large, intact quartz crystals (Fig. 6f). The identification of these opaque grains as gold was confirmed by EDS analysis in the ESEM.

4.2.3. Silica-listvenite (Birbirite)

The birbirite is composed essentially of quartz (77.4–91.1 vol%); the balance is made up of carbonates and minor opaque minerals.

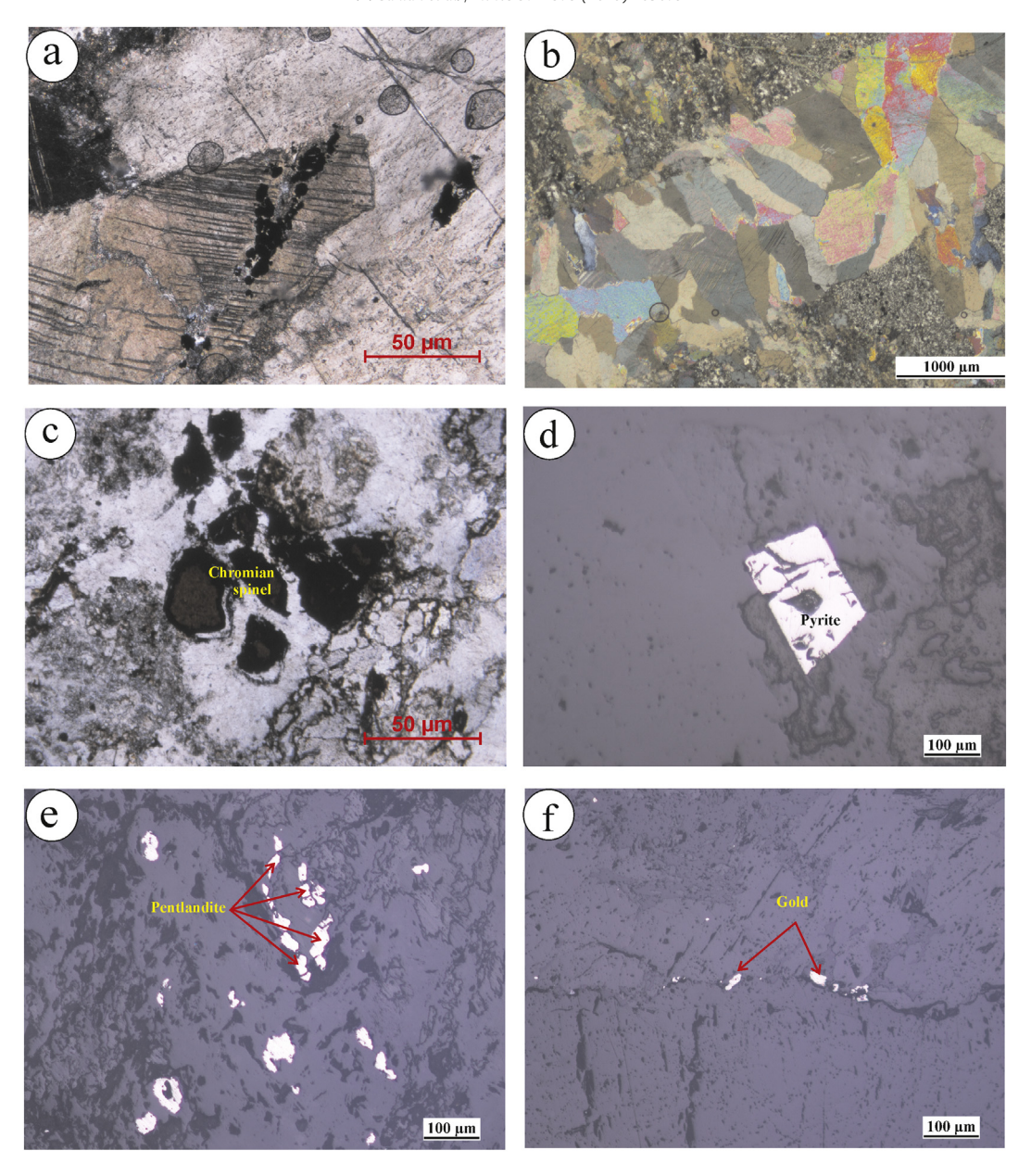


Fig. 5. Photomicrographs showing petrographic textures of carbonate listvenite under plane-polarized transmitted light (a and c), crossed nicols (b) and reflected light (d, e and f): (a) coarse-grained crystals of magnesite with well-formed cleavage; (b) dolomite vein crosscutting fine-grained carbonates; (c) reddish brown cracked crystal of Cr-spinel; (d) euhedral crystal of pyrite; (e) anhedral grains of pentlandite randomly scattered within the carbonate listvenite; and (f) fine specks of gold along fractures. (For interpretation of the references to color in this figure legend, the reader is referred to the web version of this article.)

Pseudomorphic ghost-textures after serpentine (mesh and bastite) are observed in a few samples. Quartz occurs as subhedral to euhedral, fine- to medium-grained, interlocking crystals in a mosaic texture (Fig. 7a). Silica also occurs as minor microcrystalline chalcedony veins. The birbirite contains minor carbonate fracture fillings as well as sparse large rhombs of dolomite that have been mostly replaced by fine aggregates of late microcrystalline silica. Some birbirite outcrops contains thin bands rich in muscovite (Fig. 7b).

Birbirite is very poor in opaque minerals. In polished sections where any opaques are present at all, they are mainly sulfides with minor Crspinel and gold. Pyrite and rare chalcopyrite are the main sulfide minerals, found as fracture-filling, disseminated, fine euhedral cubes (Fig. 7c) and as small relics in the core of colloform geothite (Fig. 7d). Cr-spinel forms small, brecciated and fractured crystals associated

with carbonate (Fig. 7e). Minute specks of gold are found in birbirite, associated with sulfides (Fig. 7f).

5. Mineral chemistry

Microprobe and EDS analysis were used to confirm petrographic identification of the essential and accessory minerals. However, not all observed mineral phases were suitable for microprobe analysis, either because of small size or due to the limited number of elements that can be analyzed in a practical protocol. Microprobe data are presented for olivine, pyroxene, chlorite, fuchsite, talc, tremolite, Cr-spinel and carbonates. Sulfides and gold were analyzed semi-quantitatively by EDS and are shown normalized to 100%. The complete mineral chemistry dataset is given in the Electronic Appendix (Supplementary Tables S1-S10).

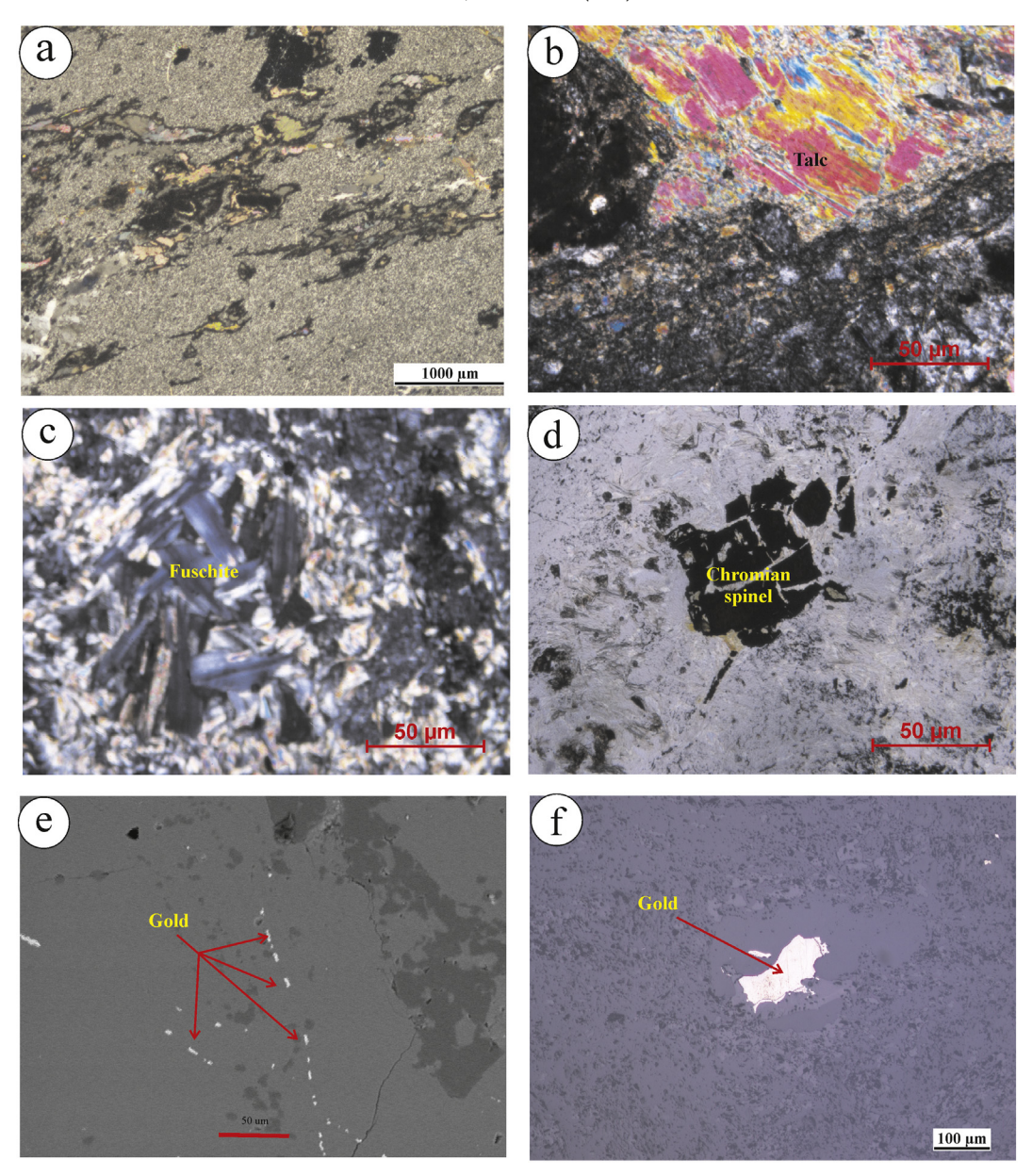


Fig. 6. Photomicrographs showing petrographic textures of silica-carbonate listvenite under plane-polarized transmitted light (a and d), crossed nicols (b and c), SEM backscatter (e), and reflected light (f): (a) preferred orientation and flattening of coarse carbonates within a matrix of fine-grained silica and carbonates; (b) large plate and fine-grained aggregates of talc; (c) fuchsite filling a cavity; (d) anhedral cracked crystal of Cr-spinel with deep blood color; (e) fine specks and blebs of gold along fractures in quartz; and (f) gold inclusion within quartz crystal. (For interpretation of the references to color in this figure legend, the reader is referred to the web version of this article.)

5.1. Silicate minerals

The analyzed silicate minerals include olivine, pyroxene, fuchsite, talc, tremolite and chlorite. Fresh olivine relics were recorded and analyzed only in serpentinite. Chemical compositions, calculated structural formulae, and end-member components are given in Supplementary Table 1. Olivine relics are unzoned and exhibit a relatively narrow range of forsterite contents (91–93, average 92), consistent with recently published data on Ess serpentinite by Gahlan et al. (2020a). The high Fo and NiO contents (0.32–0.53 wt%) resemble those of primary mantle olivines (e.g. Coish and Gardner, 2004; Pearce et al., 2000).

Some of the rare fresh relics of clinopyroxene and orthopyroxene in serpentinite were analyzed; chemical compositions and structural formulae of the analyzed pyroxenes are listed in Supplementary Table 2. The clinopyroxene exhibits limited variation in its composition; it is identified mainly as diopside according to the nomenclature of

Morimoto et al. (1988). It has Mg# between 0.90 and 0.94, with an average 0.92. The orthopyroxene, also rather homogeneous in composition, is classified mainly as enstatite (Morimoto et al., 1988), and has Mg# between 0.91 and 0.93 with an average of 0.92. The similar Mg# of olivine and orthopyroxene relics in the serpentinite suggest that these two phases might have equilibrated under high-temperature mantle conditions (Uysal et al., 2016). The orthopyroxene has Al_2O_3 (1.2–1.7 wt%) and CaO (0.9–1.3 wt%) contents similar to those of primary mantle orthopyroxenes (Ishimaru et al., 2007).

Fuchsite was analyzed in both carbonate and silica-carbonate listvenites; chemical compositions and structural formulae are given in Supplementary Table S3. All the fuchsite analyses show elevated Cr_2O_3 (4.3 to 7.8 wt%), with fuchsite from carbonate listvenite notably lower in Cr_2O_3 (4.3–5.3 wt%) than that from silica-carbonate listvenite (5.0–7.8 wt%). NiO contents mostly are below 0.6 wt%. In most cases, concentrations of Na_2O are less than 1.0 wt%. K_2O contents are variable,

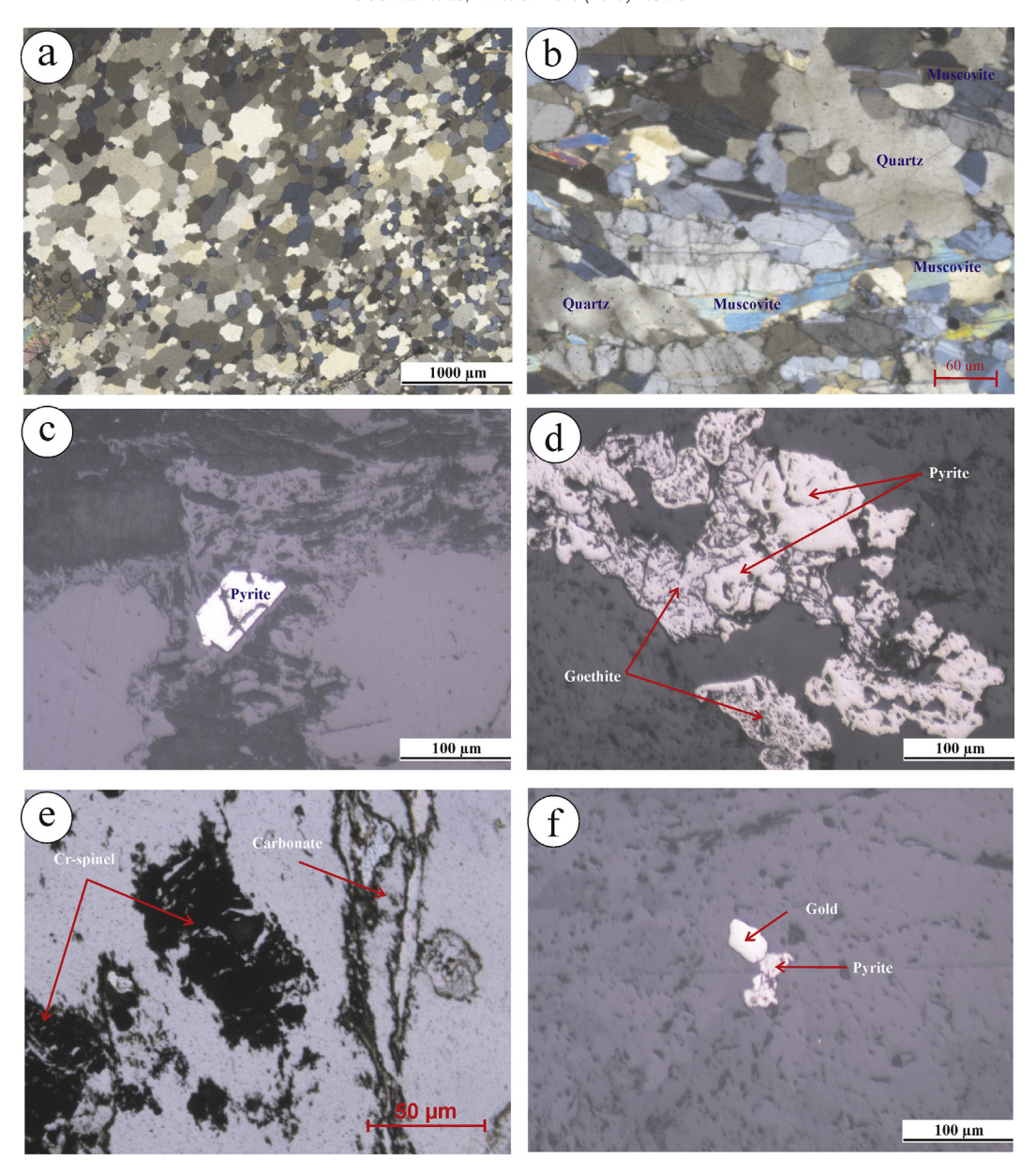


Fig. 7. Photomicrographs showing petrographic textures of birbirite under plane-polarized transmitted light (e), crossed nicols (a and b) and reflected light (c, d and f): (a) interlocking quartz crystals forming mosaic texture; (b) muscovite-rich band in birbirite; (c) disseminated pyrite crystals; (d) small relics of pyrite within goethite; (e) fractured crystals of Cr-spinel; and (f) gold grain associated with pyrite.

between 6.8 and 10.1 wt%. All fuchsite analyses are very close to dioctahedral stoichiometry, with 4.02 to 4.16 (average 4.09) octahedral cations per 24-oxygen formula unit. Compared to an ideal $K_2(Cr+Al)_4$ (Al $_2Si_6$)O $_2O(OH)_4$ formula, the excess tetrahedral charge due to Si^{IV} apfu between 6.38 and 6.51 (average 6.46) is balanced roughly equally by charge deficits due to divalent octahedral cations and to A-site vacancies.

Grains of talc, large enough to analyze, are only found in silica-carbonate listvenite; chemical and structural formulae are given in Supplementary Table S4. Talc is dominated by SiO_2 (60.6-62.2 wt%) and MgO (27.9-29.3 wt%), with minor NiO (1.3-2.4 wt%) and FeO (1.8-2.1 wt%) contents.

Chlorite analyses are reported for all the studied rock types; oxide analyses and structural formulae based on 28-oxygen formula units are in Supplementary Table 5. All chlorite analyses have high MgO, Al₂O₃ and FeO contents and low SiO₂. According to Hey (1954), chlorite in the Ess listvenites is classified mainly as clinochlore with less

penninite. The chlorite in serpentinite is more variable in composition and nomenclature. The chlorite in aureoles around Cr-spinel is the Cr-bearing variety informally known as kämmererite, with higher $\rm Cr_2O_3$ (3.13–4.01 wt%) and MgO (21.93–23.35 wt%) than disseminated chlorite (0.98–1.91 wt% $\rm Cr_2O_3$ and 15.52–21.25 wt% MgO). Formally, Cr-rich chlorite in serpentinites is classified mainly as ripidolite, whereas disseminated chlorite includes pycnochlorite and ripidolite.

Amphibole was observed and analyzed only in serpentinite; chemical compositions and structural formulae are in Supplementary Table 6. All amphibole is calcic and classified as tremolite according to Leake et al. (1997); this is consistent with its petrographic occurrence as a secondary phase after primary pyroxenes and olivine.

5.2. Non-silicate minerals

The analyzed non-silicate minerals include Cr-spinel, carbonates, sulphides, and gold. Chemical analyses and structural formulae of

accessory Cr-spinel and its alteration products in listvenites and serpentinite are listed in Supplementary Table 7. In most analyzed Crspinel crystals, Cr₂O₃, Al₂O₃ and MgO show a systematic decrease from core to rim, whereas FeO^T increases outwards. Ferritchromite rims are enriched in total FeO and MnO, but depleted in Al₂O₃ and MgO, compared to fresh Cr-spinel. The Cr-spinel in serpentinite has Cr# between 0.65 and 0.70 with an average of 0.68, while Mg# ranges between 0.52 and 0.60 with an average of 0.57. The Cr# of Cr-spinels in the listvenites is 0.60-0.63 in both carbonate and silica-carbonate listvenite and 0.60 in birbirite. The Mg# of fresh Cr-spinels in the listvenites displays a wider range (0.53–0.60 in carbonate listvenite, 0.39–0.56 in silica-carbonate listvenite and 0.39–0.52 in birbirite). The decrease in Mg# of Cr-spinel from serpentinite through carbonate listvenite to birbirite suggests progressive re-equilibration of Cr-spinel at each stage of listvenitization. Ferritchromite rims in the carbonate and silica-carbonate listvenites have low Mn content compared to those in birbirite and serpentinite due to favorable uptake of Mn by carbonate minerals (Deer et al., 1992).

MgO, CaO, FeO^T, and MnO analyses by electron probe in carbonate minerals are listed in Supplementary Table 8; totals are not quantitative because CO₂ is not counted. The analyzed carbonates include mainly magnesite and ferroan magnesite (breunnerite); calcite and dolomite are less common. Magnesite is the main carbonate mineral in both serpentinite and listvenite. Its cation content is dominated by MgO, with CaO < 0.46 wt%, MnO < 0.64 wt%, and FeO^T < 4.3 wt%. Points classified as breunnerite have 7.5-13.5 wt% FeOT, while CaO remains < 0.79 wt% and MnO < 1.03 wt%. MgO and FeO^T are negatively correlated among the breunnerite analyses (Fig. 8), with a general trend of increasing MgO and decreasing FeOT from the serpentinite samples through silica-carbonate listvenite to carbonate listvenite. Dolomite is observed only in carbonate and silica-carbonate listvenites; it is dominated by MgO (19.6-21.7 wt%) and CaO (30.7-32.2 wt%). Calcite is recorded in carbonate listvenite, silica-carbonate listvenite and serpentinite. It consists essentially of CaO (53.6-56.9 wt%) with minor amounts of MgO (0.1-1.8 wt%) and FeO^T (0.1-0.3 wt%).

Sulfide minerals were analyzed semi-quantitatively in listvenites and serpentinite by EDS on the ESEM, for the purpose of phase identification to discriminate between the sulfide phases found in each rock type. The normalized chemical analyses are given in Supplementary Table 9. The observed sulfide minerals include pyrite, arsenopyrite, chalcopyrite, sphalerite and pyrrhotite. Pyrite has low As (\leq 1.5 atomic wt%). Arsenopyrite is recognized by high As (\geq 42.3 wt%) and Fe (>34.25 wt%), chalcopyrite by high Cu (\geq 34.6 wt%) and Fe (28.01

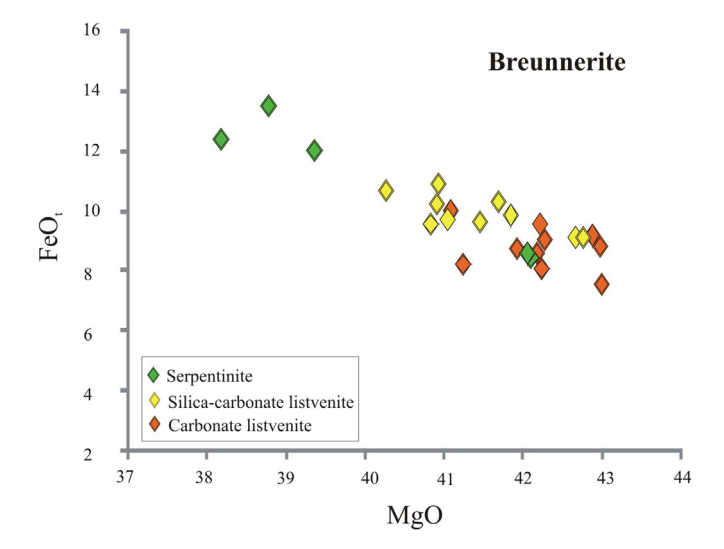


Fig. 8. MgO vs. FeO_t for breunnerite in the Jabal Ess serpentinite and listvenites.

wt > %), sphalerite by high Zn (57.7–61.9 wt%) with appreciable Fe (9.4–11.2 wt%), and pyrrhotite by Fe (57.6–59.7 wt%) and S (39.2–40.7 wt%) contents consistent with Fe/S ratios approaching unity.

Several nuggets of native gold were analyzed by EDS in each of the listvenite varieties. Their normalized analyses are given in Supplementary Table S10. They are composed mainly of Au (77.97 to 86.33%) and Ag (13.45–21.73%) with minor Fe (0.02–1.49%). The calculated gold fineness $[1000^*\text{Au}/(\text{Ag} + \text{Au})]$ of the nuggets ranges from 782 to 865, with an average of 836.

6. Geochemistry

Whole-rock chemical analyses of samples of the three listvenite varieties are given in Table 1 and those of the associated serpentinized peridotite in Table 2.

The chemical composition of the Jabal Ess serpentinite is quite typical among ophiolitic serpentinites in the Arabian Shield (e.g. Abuamarah et al., 2020; Gahlan et al., 2020b). The concentrations of TiO $_2$ (<0.1 wt%), Al $_2$ O $_3$ (<0.8 wt%), CaO (0.3–1.2 wt%), K $_2$ O (<0.01 wt%) and Na $_2$ O (<0.02 wt%) are all quite low; the analyses are dominated by SiO $_2$ (36.8–39.0 wt%), MgO (36.8–41.7 wt%), Fe $_2$ O $_3$ (7.6–8.5 wt%), and LOI (12.8–15.5 wt > %). The whole-rock Mg# of serpentinites (0.90–0.91, av. 0.90) is consistent with oceanic peridotites (Mg# >0.89; Bonatti and Michael, 1989) and other strongly depleted, harzburgite-derived serpentinites in the Arabian Shield.

As expected from the major petrographic differences, the three varieties of listvenite show significantly different abundances of all major oxides and of volatile contents (LOI). On a SiO_2 -Fe $_2O_3$ -(MgO + CaO) ternary diagram (Fig. 9a), the listvenite categories, already distinguished in the field and petrographically, are plainly separated; the silicacarbonate listvenite samples plot between the carbonate listvenite and birbirite groups. The birbirite samples contain some Fe₂O₃ and plot along the SiO₂ - Fe₂O₃ edge of the ternary. In MgO and CaO variation diagrams versus silica (Fig. 9b, c), the trend from serpentinite to carbonate listvenite is marked by a decrease in SiO₂ and MgO and a large increase in CaO content. Then from carbonate listvenite through silica-carbonate listvenite to birbirite there is an obvious trend of decreases in both MgO and CaO as the analysis becomes dominated by SiO₂. The high MgO values in carbonate-rich and silica-carbonate listvenites are entirely consistent with the dominance of magnesite among the carbonate minerals in these samples, as commonly found in listvenites worldwide (e.g. Hinsken et al., 2017). However, it is important to note that the transformation of serpentinite to magnesite-rich carbonate listvenite is accompanied by a substantial net loss of MgO. The gain in CaO content from serpentinite to carbonate listvenite is consistent with the development of calcite and dolomite as a component of the carbonate mineral assemblage.

There is also a good positive correlation between MgO and loss on ignition (LOI) among listvenites (Fig. 9d), implying that the volatile budget of listvenite is dominated by CO₂ in the form of Mg-rich carbonates. Serpentinites do not plot on the same correlation line in Fig. 9d because LOI in serpentinites is dominated instead by H₂O in serpentine; the loss of water mass exceeds the gain in CO₂ mass, resulting in a decrease of LOI from serpentinite to carbonate listvenite. A few samples classified as birbirite have relatively high LOI (up to 3.6 wt%) and CaO content (up to 4.9 wt%) due to the presence of minor calcite. The total iron in birbirite samples is somewhat elevated (6.0-12.3 wt%, av. 8.5 wt%) relative to other listvenites (4.7-6.7 wt%, av. 5.8 wt% in carbonate listvenite; 3.0-5.6 wt%, av. 4.0 wt% in silica-carbonate listvenite). Total Fe₂O₃ in birbirite is coincidentally similar to that in serpentinites (8.3–9.6 wt%, av. 9.0 wt%), but the elevated Fe in birbirite is attributed to the presence of supergene iron oxides. Other oxides (Al₂O₃, TiO₂, Na₂O, K₂O, and MnO) are very low in all listvenite varieties and do not show any significant correlations with the major oxides. However, the silica-carbonate listvenite samples containing visible fuchsite under

Table 1Major, trace and REE contents in the listvenites of Jabal Ess.

Rock type	Carbonate listvenite													
Sample No	ES4	ES13	ES17	Е	S19	ES25	ES28	ES36	ES43	ES5	4	ES57	ES66	ES73
SiO ₂	28.42	24.76	26.34	1 2	4.52	27.4	26.31	25.01	30.21	25.	23	28.12	29.03	26.75
TiO ₂	< 0.01	0.02	< 0.0		.01	0.01	0.01	< 0.01	< 0.01	0.0		< 0.01	< 0.01	0.01
Al_2O_3	1.12	0.41	0.47		.16	0.28	0.09	0.25	0.91	0.2		0.14	1.24	0.48
Fe ₂ O ₃	6.25	6.67	6.68	4	.73	5.99	6.2	5.42	5.5	5.1	5	5.79	5.29	5.83
MnO	0.11	0.09	0.1	0	.08	0.06	0.12	0.09	0.07	0.1	4	0.1	0.11	0.08
MgO	24.54	25.03	26.26		6.51	29.36	29.12	24.38	27.27	25.		26.61	23.49	28.64
CaO	9.31	10.97	9.91		.91	7.68	8.69	11.42	7.39	9.9		8.38	10.72	9.59
$N_{a2}O$	0.01	< 0.01	< 0.0		.01	< 0.01	< 0.01	0.01	0.02	<0.		< 0.01	0.01	0.01
K ₂ O	0.56	0.21	0.17		.24	0.13	0.22	0.18	0.67	0.1		0.14	0.81	0.17
P_2O_5	0.01	0.02	< 0.0		.01	< 0.01	0.02	< 0.01	0.03	<0.		0.01	< 0.01	0.01
LOI	29.8	31.23	29.83		3.83	29.08	29.17	33.28	28.31	32.		30.32	30.01	28.28
Total	100.13	99.41	99.76		00.01	99.99	99.95	100.04	100.38			99.61	100.71	99.85
Sc	5.5	6	6.5	2	.4	4.5	3.5	5.7	5.2	3.7		3.7	4.1	5.7
Ва	23.5	16.3	17.3		2.8	26.5	34.1	27.4	94.5	37.		27.8	55.2	26.6
Ве	<1.0	<1.0	1.4	1		1.3	1.2	1.1	<1.0	<1.		1	1.8	1.1
Ni	1585	1993	1863		076	1852	979	1040	1320	143		1016	1303	1651
Co	90.2	90.2	89.1		3.2	86.4	97.4	84.8	62.5	70.		83.7	77.9	79.6
Cs	< 0.1	< 0.1	< 0.1		.1	0.2	< 0.1	0.2	0.1	<0.		< 0.1	< 0.1	0.3
Ga	1.1	0.7	0.9		.5	0.7	0.6	1.1	1.2	0.8		1.1	1.2	0.9
Hf	0.2	<0.1	0.3		.5 :0.1	0.7	0.0	0.2	0.1	<0.		<0.1	<0.1	<0.1
Nb	<0.1	0.1	0.1		(0.1	0.1	0.1	<0.1	0.1	0.2		<0.1	<0.1	<0.1
Rb	0.2	<0.1	0.1		.1	0.5	<0.1	<0.1	0.6	0.2		0.1	<0.1	<0.1
Sn	0.2	0.8	1		.1 .9	10.9	1.2	1.3	0.8	1.1		1.6	0.8	1.1
Sr	277.6	105.2	1 124.3		.9 50.4	98.5	1.2 199.2	469.7	303.8	1.1		334.5	0.8 277.9	1.1
Ta	0.1	<0.1	<0.1		0.1	0.1	<0.1	0.1	0.4	0.1		0.2	0.3	0.1
Th	< 0.1	0.2	<0.1		:0.1	0.2	<0.1	0.1	0.1	<0.		<0.1	<0.1	< 0.1
U	< 0.1	0.2	0.1		0.1	0.1	<0.1	0.1	0.2	0.2		<0.1	<0.1	< 0.1
V	28.5	38	35.1		.2	19.5	22.7	16.7	47.5	27.		15.6	22.3	24.3
W	2.3	2.3	2.6		.5	2.3	0.9	0.8	1.4	1.7		0.6	0.5	2.1
Zr	2.3	12.3	1.5		.6	2.1	1.5	2.1	1.6	2.2		1.7	1.6	1.9
Y	0.3	0.6	0.4	0.	.1	0.3	0.2	< 0.1	1.2	0.1		0.2	0.1	0.2
Mo	0.2	0.1	< 0.1	0.	.1	< 0.1	0.2	0.2	< 0.1	0.3		0.1	0.2	0.1
Cu	85.9	25.8	24.6		5.6	3.4	67.9	41.4	85.9	22.	3	36.8	41.7	86.9
Pb	45.7	0.3	6.3	1.	.4	2.5	156.7	8.8	369.5	1.9		54.6	4.5	71.8
Zn	562	5.3	173.3		5.5	4	192.3	92.5	266.3	11.		77.1	70.7	237.2
As	338.5	39.4	86.7		.1	132.5	203.4	13.3	633.8	11.		2.9	12.1	744.1
Cd	0.6	0.2	0.5		:0.1	<0.1	<0.1	0.2	<0.1	<0.		0.3	0.4	0.2
Sb	0.9	0.5	0.8		.4	1.9	<0.1	0.5	8.7	0.6		0.4	<0.1	5.6
Bi	0.3	<0.1	0.3		. :0.1	<0.1	0.3	<0.1	0.2	0.0		<0.1	0.2	<0.1
	1.4						2.6		3.4					
Ag		< 0.1	0.1		0.1	0.1		<0.1		0.1		0.2	<0.1	< 0.1
Au**	2538.6	34.7	39.2		.1	5	728.3	5.5	2569.2			10.1	3.6	427.5
Hg	0.31	0.21	0.18		.09	0.67	1.23	3.12	0.27	0.3		2.46	1.84	0.22
Se Cr	1.2 1506	0.4 1344	0.3 1461		.5 549	0.7 1352	0.6 1618	0.7 1556	0.4 1140	0.5 152		0.5 1008	1.4 1282	0.3 1268
Ci	1500	1344	1401	1.	343	1332	1016	1330	1140	132	.J	1008	1202	1200
La	0.19	<0.1	0.25		0.1	0.27	<0.1	<0.1	0.38	0.3		0.31	0.32	0.29
Ce	0.33	< 0.1	0.58		.11	0.62	0.09	0.23	0.92	0.4		0.64	0.32	0.65
Pr	0.04	0.04	0.09		.02	0.09	0.03	0.02	0.12	0.0		0.08	0.05	0.11
Nd	< 0.3	< 0.3	0.37		:0.3	0.42	< 0.3	< 0.3	0.11	0.4		0.34	< 0.3	0.45
Sm	< 0.05	0.13	0.11		0.05	0.12	< 0.05	< 0.05	0.18	<0.		0.07	0.12	0.13
Eu	< 0.02	< 0.02	0.04		0.02	0.04	< 0.02	< 0.02	0.07	0.2		< 0.02	0.15	0.05
Gd	< 0.05	0.19	0.16		0.05	0.14	< 0.05	< 0.05	0.21	<0.		< 0.05	0.15	0.18
Tb	< 0.01	< 0.01	0.03	<	:0.01	0.03	< 0.01	< 0.01	0.04	0.0	2	0.02	< 0.01	0.03
Dy	0.08	< 0.05	0.2		:0.05	0.18	< 0.05	< 0.05	0.3	0.0		0.13	< 0.05	0.2
Но	< 0.02	0.03	0.04		0.02	0.04	0.02	< 0.02	0.06	0.0	2	< 0.02	0.02	0.04
Er	< 0.03	0.07	0.11	0.	.03	0.1	< 0.03	0.03	0.15	<0.	03	< 0.03	0.04	0.12
Tm	< 0.01	0.02	0.01	<	0.01	0.02	< 0.01	< 0.01	0.03	<0.	01	0.02	< 0.01	0.02
Yb	< 0.05	0.08	0.1		0.05	0.11	< 0.05	< 0.05	0.17	0.0		0.05	< 0.05	0.12
Lu	< 0.01	< 0.01	0.01		0.01	0.02	0.01	< 0.01	0.03	<0.		0.01	< 0.01	0.02
Eu/Eu*			0.92			0.94			1.10					1.00
(La/Yb)n			1.69			1.66			1.51					1.63
((La/Sm)n			1.43			1.42			1.33					1.41
(Gd/Lu)n			1.96			0.86			0.86					1.10
(La/Lu)n			2.56			1.38			1.30					1.49
Rock type	Silica, carb	onate listve	nite			Birbirite								
Sample No	#ES2	#ES12	#ES23	#ES40	#ES51	\$ES7	\$ES15	\$ES20	\$ES31	\$ES38	\$ES45	\$ES59	\$ES68	\$ES75
SiO ₂	49.36*	46.69	44.23	55.15*	49.02	89.41	88.55	83.54	87.82	77.38	84.05	89.9	85.73	91.08
TiO ₂	0.01	< 0.03	0.02	< 0.01	0.03	< 0.01	0.01	0.02	< 0.01	0.02	< 0.01	< 0.01	0.01	< 0.01
1102														
Al_2O_3	1.65	0.66	0.22	1.41	1.01	0.11	0.11	0.25	0.19	0.78	0.19	0.15	0.31	0.29

(continued on next page)

Table 1 (continued)

Rock type	Silica-carbonate listvenite					Birbirite								
Sample No	#ES2	#ES12	#ES23	#ES40	#ES51	\$ES7	\$ES15	\$ES20	\$ES31	\$ES38	\$ES45	\$ES59	\$ES68	\$ES7:
MnO	0.11	0.09	0.07	0.06	0.05	0.05	0.07	0.34	0.04	0.06	0.05	0.05	0.17	0.08
MgO	18.91	20.27	19.29	16.74	18.56	0.5	1.43	0.26	0.37	0.59	1.05	0.39	0.78	0.25
CaO	6.91	7.07	7.38	5.06	6.82	0.21	0.15	2.12	1.65	4.88	1.96	0.32	3.02	0.28
Na ₂ O	0.37	0.11	0.04	0.06	0.18	0.02	< 0.01	0.03	0.01	< 0.01	0.02	< 0.01	< 0.01	0.02
K ₂ O	1.87	0.96	0.57	2.06	0.67	0.11	0.17	0.21	0.16	0.12	0.18	0.15	0.22	0.28
P_2O_5	0.05	0.07	0.02	< 0.01	0.04	0.02	0.11	0.13	< 0.01	0.01	0.05	0.08	< 0.01	0.05
LOI	18.05	20.85	22.29	15.3	18.92	1.56	1.7	2.43	1.32	3.6	2.24	1.45	3.32	1.87
Total	50.94	100.3	99.68	44.55	99.41	99.38	99.52	100.3	100.7	99.78	100.1	99.56	99.74	100.2
Sc	3.4	2.8	3.1	4.5	3.8	3.1	3.2	6.3	2.4	8.2	3	2.8	4.7	4.4
Ba	53.7	37.2	123.6	92.5	66.7	38.6	43.5	88.2	76.5	267.8	76.4	49.5	56.7	28.2
Be	<1.0	<1.0	1.1	1	1.2	1.2	1.1	1.6	1.4	1.3	<1.0	1	1.5	1.2
Ni	885	799	861	992	634	1004	1063	914	479	383	1076	987	1089	1002
Со	42.5	56.1	82.1	33.9	49.8	105.9	68.1	116.7	43.6	42.8	66.7	62.3	94.8	85.2
Cs	0.1	<0.1	0.2	0.3	<0.1	< 0.1	<0.1	<0.1	< 0.1	< 0.1	0.2	< 0.1	0.1	< 0.1
Ga	2.2	1.6	0.8	2.2	1.3	0.8	0.7	1.1	1.4	1.3	1.2	1.2	0.8	1.4
Hf	< 0.1	0.1	< 0.1	0.2	<0.1	< 0.1	0.7	<0.1	0.1	<0.1	0.1	<0.1	0.8	< 0.1
нı Nb														
	0.1	<0.1	0.2	0.1	<0.1	<0.1	0.2	0.1	<0.1	0.2	0.1	<0.1	0.1	<0.1
Rb	0.8	1.1	0.4	1.2	1.1	0.2	0.5	<0.1	0.5	0.4	< 0.1	0.4	0.1	0.3
Sn	0.7	1.1	0.9	0.6	0.8	1.1	0.9	0.6	0.8	1.2	0.7	1.2	1.1	0.7
Sr	672.8	549.6	182.1	882.7	471.8	18.2	16.9	55.6	69.5	128.8	88.5	21.1	23.6	88.1
Ta	0.1	0.1	0.2	0.5	0.3	0.1	< 0.1	0.1	0.1	< 0.1	0.1	< 0.1	0.2	< 0.1
Th	< 0.1	0.1	< 0.1	0.2	< 0.1	< 0.1	0.1	< 0.1	0.2	< 0.1	< 0.1	0.1	< 0.1	0.2
U	0.2	< 0.1	0.1	0.2	< 0.1	0.4	0.5	1.5	2.4	3.1	1.2	0.4	< 0.1	0.2
V	18	17.7	32.7	47	25.7	21.1	24.8	160.9	97.2	175.7	160.2	29.6	38	117.
W	4.2	3.3	1.2	8.9	4.4	23.2	6.8	20.8	32.9	10.7	25.9	16.6	5.1	13.6
Zr	2.5	1.8	1.5	7.1	3.2	1.8	1.2	0.7	0.8	1.4	1.1	1.4	0.8	0.6
Y	3.8	2.6	0.2	3.4	2.3	1.1	1.8	2.5	0.6	1.8	1.3	1.5	0.6	0.5
Mo	0.9	0.7	< 0.1	0.4	0.5	0.9	1.1	3.6	0.8	1.6	0.9	0.8	0.7	1.2
Cu	24.2	56.3	25.7	68.6	43.7	5.3	3.8	56.5	39.8	37.4	49.8	5.7	20.2	12.9
Pb	0.9	137.5	3.2	251.5	98.2	1.1	1.1	44.7	53.9	63.9	42.6	2.5	14.9	3.2
Zn	9	412.7	12.2	421.5	203.8	8.4	9.1	35.6	47.2	37.6	43.4	11.3	28.1	11.9
As	115.9	662.3	11.1	435.4	295.8	7.3	6.6	67.1	9.5	8.8	86.9	6.7	117.9	3.2
Cd	< 0.1	0.7	< 0.1	0.3	0.4	< 0.1	< 0.1	< 0.1	0.1	< 0.1	< 0.1	0.1	< 0.1	0.1
Sb	12.5	9.4	0.3	4.8	6.5	1.5	1.4	1.3	0.4	0.5	0.9	1.1	0.8	2.3
Bi	< 0.1	0.1	< 0.1	0.1	<0.1	<0.1	<0.1	<0.1	0.1	< 0.1	0.1	0.2	<0.1	0.1
Ag	<0.1	1.5	<0.1	2.3	1.7	0.2	<0.1	0.8	0.3	0.5	0.6	< 0.1	0.6	<0.1
Au**	417.7	2195	42.6	3117	961.1	5.3	15.1	315.6	280.6	174.3	95.8	6.7	80.3	4.7
	0.27	0.46	0.54	0.17	0.22	0.17	0.28	0.34	0.23	0.32	0.24	0.7	0.41	0.19
Hg So	0.27		3.8		0.22	0.17		0.34		0.32				1.1
Se Cr		1.2		0.6			0.8		0.5		0.4	0.5	0.6	741
Cr	1556	997	1474	1296	1108	941	470	1070	716	480	798	1010	844	
La	<0.1	0.15	<0.1	0.22	<0.1	<0.1	0.55	0.53	0.72	0.91	0.48	0.39	1.35	2.73
Ce	<0.1	0.37	<0.1	0.51	0.18	< 0.1	1.37	0.53	1.81	1.17	1.13	1.01	2.78	5.81
Pr	< 0.02	0.05	< 0.02	0.08	< 0.02	0.06	0.21	0.05	0.27	0.15	0.18	0.15	0.38	0.68
Nd	0.3	0.21	<0.3	0.34	< 0.3	0.61	0.95	<0.3	1.28	0.81	0.8	0.67	1.43	2.7
Sm	< 0.05	0.06	< 0.05	0.09	< 0.05	< 0.05	0.21	< 0.05	0.27	< 0.05	0.21	0.19	0.35	0.67
Eu	< 0.02	0.02	< 0.02	0.03	< 0.02	< 0.02	0.06	< 0.02	0.07	0.58	0.13	0.1	0.16	0.45
Gd	< 0.05	0.08	< 0.05	0.1	< 0.05	0.12	0.23	< 0.05	0.29	< 0.05	0.32	0.25	0.38	0.76
Γb	< 0.01	0.01	0.01	0.02	< 0.01	< 0.01	0.04	0.02	0.05	< 0.01	0.06	0.04	0.07	0.11
Оу	< 0.05	0.09	< 0.05	0.11	< 0.05	< 0.05	0.26	< 0.05	0.32	< 0.05	0.36	0.28	0.46	0.59
Ho	0.02	0.02	0.02	0.03	0.03	0.03	0.05	< 0.02	0.07	0.02	0.08	0.07	0.09	0.12
Er	< 0.03	0.07	< 0.03	0.08	< 0.03	< 0.03	0.15	0.06	0.18	< 0.03	0.26	0.2	0.26	0.31
Гm	< 0.01	0.01	< 0.01	0.01	< 0.01	< 0.01	0.02	< 0.01	0.03	< 0.01	0.04	0.03	0.04	0.05
Yb	< 0.05	0.07	< 0.05	0.08	< 0.05	< 0.05	0.14	< 0.05	0.19	< 0.05	0.27	0.21	0.27	0.33
Lu	0.01	0.01	0.01	0.01	< 0.01	< 0.01	0.02	< 0.01	0.03	< 0.03	0.04	0.03	0.05	0.06
Eu/Eu*	0.01	0.88	0.01	0.01	\U.U.I	\U.U1	0.83	\U.U1	0.76	\U.U1	1.53		1.34	1.93
												1.40		
(La/Yb) _n		1.45		1.86			2.66		2.56		1.20	1.26	3.38	5.59
(La/Sm) _n		1.58		1.54			1.65		1.68		1.44	1.30	2.43	2.57
(Gd/Lu) _n		0.98		1.23			1.41		1.18		0.98	1.02	0.93	1.55
(La/Lu) _n		1.54		2.25			2.82		2.46		1.23	1.33	2.77	4.66

^{*} Fuschite bearing samples.

Major elements in weight percent; trace elements in $\mu g/g$ except ** Au in ng/g.

Rare earth element ratios are left blank when one or more of the elements in question is below detection limit.

the microscope have higher contents of K_2O (1.9–2.1 wt%) and Al_2O_3 (1.4–1.7 wt%) than the other samples.

The trace element contents of the sample suite have a large dynamic range of variation. Many trace elements are at or below detection limits in all samples. Another group of elements (V, Ta, Nb, Th, Ni, Hf, Co and Cs) are present at detectable levels but show no systematic differences among sample types. Then there are a group of elements (Rb, Ba, Sr, Zn, Pb, Cu, Sb, Zr, As and Ag) that show

significantly elevated and variable concentrations in listvenites; these elements include those likely to be hosted in the abundant sulfide minerals and those likely to have been delivered by fluids during or after the listvenitization process. Au contents are also variable and highly enriched in listvenites (43–3117 ng/g in silica-carbonate listvenite, 4–2539 ng/g in carbonate listvenite and 5–316 ng/g in birbirite), compared to serpentinite (0.5 to 1.7 ng/g). The samples with the highest Au content also have the highest contents of Zn,

Table 2Major, trace and REE contents in the serpentinite of Jabal Ess ophiolite.

iviajoi, trace and	u KLL COIII	ciits iii tiic	3CI PCIIIII	ite oi jabai	L33 OPIIIO	iiic.	
Sample No	ES33	ES47	ES61	ES63	ES70	ES 78	ES80
SiO_2	38.08	37.91	36.96	37.87	39.04	38.74	36.84
TiO ₂	< 0.01	0.01	< 0.01	0.01	< 0.01	0.02	0.01
Al_2O_3	0.75	0.69	0.69	0.81	0.54	0.54	0.68
Fe_2O_3	8.04	8.08	7.61	7.85	8.51	8.01	8.08
MnO	0.08	0.09	0.12	0.14	0.11	0.07	0.1
MgO	38.76	37.43	37.28	38.74	36.76	38.73	41.70
CaO	1.17	0.91	1.02	0.34	0.62	0.52	0.56
Na ₂ O	0.01	< 0.01	0.01	< 0.01	0.01	0.02	0.02
K ₂ O	0.01	< 0.01	0.01	< 0.01	< 0.01	0.01	< 0.01
P ₂ O ₅	0.01	< 0.01	< 0.01	0.01	< 0.01	0.01	0.02
LOI	13.35	14.45	15.45	14.21	13.91	13.03	12.75
Total	100.26 0.91	99.57 0.90	99.15 0.91	99.98 0.91	99.5 0.90	99.7	100.76 0.91
Mg#	0.91	0.90	0.91	0.91	0.90	0.91	0.91
Sc	8.5	7.1	6.2	8.9	8.5	8.1	6.8
Ba	5.2	8.3	6.3	6.5	1.4	6.6	2.8
Be	<1.0	<1.0	1	<1.0	1.1	0.3	1.3
Ni	2271	2175	1993	2344	2203	2245	2131
Co	103	100	90	120	99	104	112
Cs	< 0.1	0.1	< 0.1	0.2	< 0.1	0.1	0.2
Ga	1.1	0.9	0.7	1.1	0.8	1.2	1.5
Hf	0.1	< 0.1	0.2	< 0.1	< 0.1	0.1	< 0.1
Nb	0.1	< 0.1	0.2	0.1	< 0.1	< 0.1	0.1
Rb	< 0.1	0.2	< 0.1	< 0.1	0.1	0.2	0.4
Sn	0.5	0.7	0.4	0.3	0.6	0.3	0.7
Sr	14.4	11.8	5.2	11.5	7.8	8.9	7.5
Ta	<0.1	<0.1	<0.1	<0.1	<0.1	<0.1	< 0.1
Th	0.1	<0.1	0.2	<0.1	<0.1	0.2	0.1
U V	0.1	0.2	0.1	0.1	0.2 31.6	0.1	0.2
v W	36.5 1.9	34.5 2.1	38 2.3	51.2 2.6	0.8	24.8 0.6	26.1 1.2
vv Zr	0.2	0.2	0.6	0.5	0.8	0.6	1.2
Y	0.2	<0.1	0.3	<0.1	0.2	0.4	0.2
Mo	<0.1	0.1	<0.1	0.1	0.2	<0.1	< 0.1
Cu	4.4	4.6	5.8	11.1	2.7	4.8	3.6
Pb	3.9	2.7	0.3	1.2	0.4	0.2	0.3
Zn	9.6	12.5	14.3	11.5	23.6	33.1	23.9
As	19.5	17.4	20.4	11.1	8.5	9.6	8.7
Cd	< 0.1	< 0.1	< 0.1	0.1	< 0.1	< 0.1	< 0.1
Sb	1.2	0.7	0.5	0.1	0.2	0.4	0.5
Bi	< 0.1	0.1	< 0.1	< 0.1	< 0.1	0.1	0.1
Ag	0.1	< 0.1	0.1	< 0.1	< 0.1	< 0.1	< 0.1
Au*	0.7	1.1	1.7	0.7	0.5	0.8	1.3
Hg	0.02	0.06	0.05	0.07	0.02	0.03	0.04
Se	0.2	0.3	0.5	0.4	0.2	0.3	0.2
Cr	1445	1596	1615	1548	1164	1347	1941
La	< 0.1	< 0.1	0.13	0.2	< 0.1	< 0.1	0.17
Ce	0.12	<0.1	0.13	0.2	<0.1	<0.1	0.17
Pr	< 0.02	0.02	0.23	0.06	0.03	<0.02	0.05
Nd	<0.3	< 0.3	<0.3	0.27	0.31	<0.3	0.22
Sm	< 0.05	0.05	< 0.05	0.06	< 0.05	< 0.05	0.05
Eu	< 0.02	< 0.02	< 0.02	0.02	< 0.02	< 0.02	0.01
Gd	< 0.05	0.05	< 0.05	0.06	< 0.05	< 0.05	0.05
Tb	< 0.01	< 0.01	0.01	0.01	< 0.01	< 0.01	0.01
Dy	< 0.05	0.06	< 0.05	0.07	< 0.05	< 0.05	0.07
Но	0.02	< 0.02	< 0.02	0.02	0.02	< 0.02	0.02
Er	< 0.03	0.03	0.04	0.05	< 0.03	< 0.03	0.06
Tm	< 0.01	< 0.01	0.01	0.01	< 0.01	< 0.01	0.01
Yb	< 0.05	< 0.05	< 0.05	0.06	< 0.05	< 0.05	0.07
Lu	< 0.01	0.01	< 0.01	0.01	< 0.01	< 0.01	0.01
Eu/Eu*				1.02			0.61
(La/Yb) _n				2.25			1.64
(La/Sm) _n (Gd/Lu) _n				2.10 0.74			2.15 0.49
$(La/Lu)_n$				2.05			1.39
\							

Major elements in weight percent; trace elements in $\mu g/g$ except * Au in ng/g. Rare earth element ratios are left blank when one or more of the elements in question is below detection limit.

Pb, Cu, Ag and As. There is a remarkable enrichment in Ba, Sr, Cu, Pb, Zn and V in the birbirite.

The average primitive mantle-normalized trace element pattern (normalization values of McDonough and Sun, 1995) of each rock

variety studied is shown in Fig. 10a. Generally, all the patterns show slight to moderate enrichment in large ion lithophile elements (LILE = K, Rb, Sr, Ba, U, Th) and relative depletion in high field strength elements (HFSE = Nb, Ta, Ti, and Y). The birbirites have higher concentrations of almost every trace element than the other listvenites and the serpentinites.

The chondrite-normalized rare-earth element (REE) patterns (normalization values of Evensen et al., 1978) of all the analyzed samples are shown in Fig. 10b. The REE abundances are generally low in all samples but vary by about an order of magnitude across the sample suite, with serpentinites having the lowest concentrations and birbirite the highest (Tables 1, 2). Birbirite has \sum REE concentrations from 3.62–15.37 µg/g (av. 7.86 µg/g), carbonate listvenite has 2.1–2.77 µg/g (av. 2.37 µg/g), silica-carbonate listvenite has 1.22–1.71 µg/g (av. 1.47 µg/g), and serpentinite has 1.2–1.34 µg/g (av. 1.27 µg/g). There is a slight enrichment in LREE relative to HREE (La_N/Yb_N = 1.20–3.38). The REE patterns of birbirites typically have small to moderate Eu anomalies, which may be either positive or negative [(Eu/Eu* = 0.76–1.93)].

7. Discussion

The term "listvenite" was commonly used by Soviet geologists to describe highly carbonated, sericitized and pyritized mafic and ultramafic rocks that occur in the Ural goldfields (Boyle, 1979). Due to the initial translation from Russian to different languages, a diversity of spellings of the term "listvenite" appear in the geological literature, including "listwanite", "listwaenite", "listvanite" and "listvenite". In the present work, we use the spelling "listvenite," which we judge to be the most correct rendering in English. Some authors used the term "silica-carbonate" instead of listvenite. The two terms are synonymous and encompass all forms of carbonatization and silicification from the carbonaterich to silica-rich phases (Buckman and Ashley, 2010). In general, listvenite is a term used for carbonated meta-ultramafic rocks that commonly bear fuchsite-quartz-carbonate mineral parageneses and represent the end products of various degrees of carbonatization, potassium alteration, and silicification (e.g, Azer, 2013; Gamal El Dien et al., 2019; Halls and Zhao, 1995). During the listvenitization process, primary ferromagnesian silicate minerals in ultramafic rocks are replaced by carbonate minerals and the released silica may be either mobilized out of the rock by fluids or precipitate locally as quartz (Uçurum, 2000; Azer, 2013; Gahlan et al., 2018).

7.1. Element mobility during serpentinization and listvenitization

The whole rock geochemical data from the Jabal Ess and elsewhere indicate that the transformation of serpentinite into listvenite involves profound metasomatic modification of the bulk-rock geochemistry. The chemical changes during alteration of serpentinite to listvenite are dominated by the addition of CO₂, the removal of H₂O, and the redistribution of SiO₂, MgO and CaO from serpentine intofrom serpen carbonate minerals and silica. All the listvenites at Jabal Ess are enriched in CaO, Na₂O and K₂O, but depleted in MgO compared with associated serpentinite that is presumed to represent their protoliths. Alteration also caused redistribution of trace elements, with some being locally remobilized within the rock, some being added from a fluid phase, and others being leached out of the rock. The gains and losses of elements in the studied listvenites are summarized in Fig. 11, where the average trace element abundances of the three classes of listvenite are normalized to the average abundance in the associated serpentinites. A number of first-row transition elements (Sc, Co, Ni, and Cr) are modestly and equally depleted, with serpentinite-normalized abundances of 0.3 to 0.9 in all listvenite types (thesethese are particularly invariant in the carbonate listvenite). It is likely that these elements were immobile during listvenitization and that their modest depletion indicates dilution in concentration due to addition of carbonate mass to the rock.

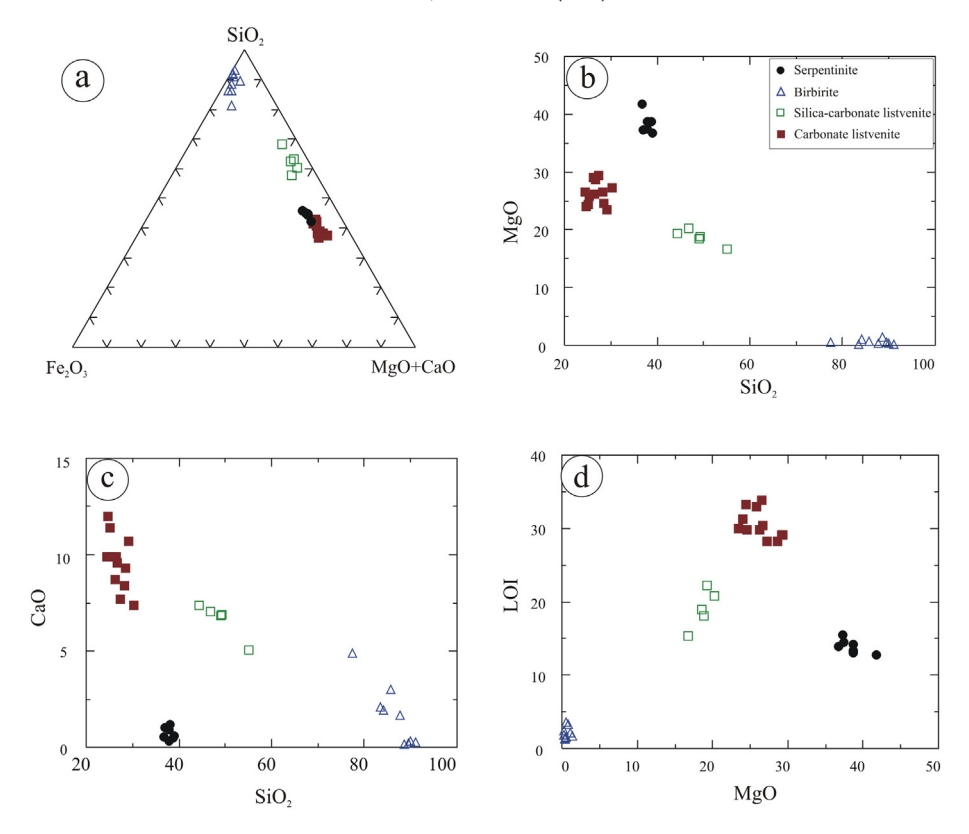


Fig. 9. Whole-rock major element chemical compositions of the Ess serpentinite and listvenites: (a) SiO₂-Fe₂O₃-(MgO + CaO) ternary diagram; (b) SiO₂ vs. MgO; (c) SiO₂ vs. CaO; and (d) MgO vs. LOI.

On the other hand, listvenites are strongly enriched relative to serpentinite in most elements that are considered to be fluid-mobile (K, As, Sr, Sb, Ba, and Pb), suggesting contributions captured from the fluid and incorporated into carbonates or silica. Some other elements that are nearly equal in carbonate listvenite and serpentinite (Rb, U and Cs) are generally considered fluid-mobile and so the absence of enrichment is surprising. The most fluid mobile elements may have simply moved through the open system during listvenitization and not accumulated in the solid products. For many elements (K, As, Zn, Pb, Au, Ag) there is a systematic behavior whereby, although all listvenite varieties are enriched relative to serpentinite, the birbirite average is least enriched, the carbonate listvenite average is intermediate, and the silica-carbonate listvenite average is most enriched.

Enrichment of precious metals in this setting is of particular interest. Gold shows similar behavior, to some extent, to the fluid-mobile elements, with maximum enrichment in the silica-carbonate listvenites, but the degree of enrichment over serpentinite is larger than that of any other component (except CO₂). Compared to serpentinite (0.5–1.7 ng/g), the Ess listvenites show much higher concentrations of Au (4–2569 ng/g in carbonate listvenite, 43–3117 ng/g in silicacarbonate listvenite and 5–281 ng/g in birbirite), suggesting that Au (as well as As, Ag, Zn, Pb, and Cu) was transferred from fluids to the solid alteration products during intense alteration of the serpentinites. Evidently, carbonation of serpentinite concentrates gold in the alteration products to grades that may well reach economic proportions. The listvenite samples that are rich in gold also contain abundant sulfides. This suggests both that gold mobilization and transportation in the fluid is associated with complexation with sulfur and that crystallization of solid sulfides provides a host to immobilize and concentrate Au and associated metals.

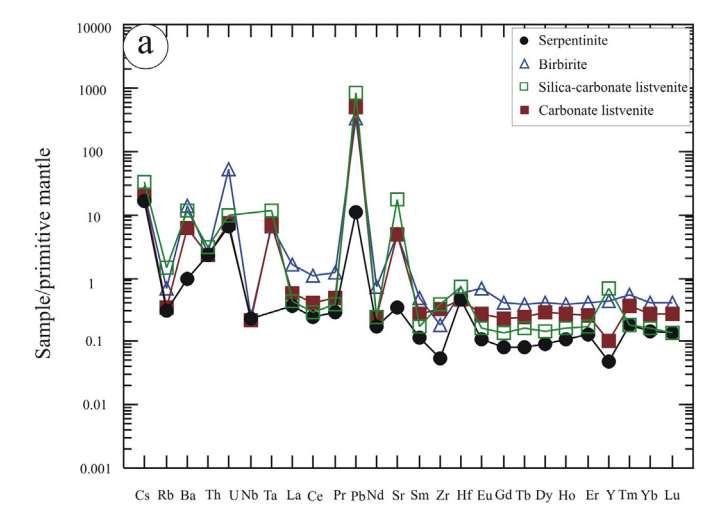
The current results are consistent with those of numerous studies worldwide that have demonstrated listvenite-hosted Au mineralization (e.g. Belogub et al., 2017; Buisson and Leblanc, 1987; Uçurum, 2000;

Uçurum and Larson, 1999), including specifically other localities in the Arabian shield (Al Jahdali, 2004; Al Jahdali et al., 2003; Harbi et al., 2006) and the Nubian shield (e.g. Azer, 2013; Botros, 2002; Osman, 1995; Ramadan et al., 2005; Zoheir and Lehmann, 2011).

7.2. Alteration of Cr-spinel to ferritchromite and kämmererite

Relics of Cr-spinel in silica-carbonate listvenite and serpentinite samples have higher Mg# than those in carbonate listvenite and birbirite (Fig. 12). This indicates that Mg-Fe²⁺ exchange affected spinel compositions during the phase of listvenitization involving quartz formation. On the other hand, the Cr-spinels in carbonate listvenite and in serpentinite are both homogeneous in the cores, with equal and high Mg#. This implies preservation of a high-temperature signature in the Mg# of Cr-spinel in carbonate listvenite. We suggest that spinels do not readily exchange Fe and Mg with carbonate minerals, whereas they do exchange with silicate phases. Hence early carbonation removed reservoir phases for Cr-spinel to exchange Fe and Mg within the carbonate listvenite, but the return of silica to the assemblage in silica-carbonate listvenite and birbirite allowed Fe—Mg exchange to resume at lower temperature. However, all the listvenite varieties have lower Cr# in their spinel cores than those in the serpentinite; this may reflect Cr—Al redistribution at lower temperature in listvenite than in serpentinite, associated with formation of either ferritchromite rims or chlorite (see below). The similar Cr# and Mg# in silica-carbonate listvenite and birbirite indicating that these two lithologies likely experienced similar cooling paths during the late alteration stage.

Most Cr-spinel in both serpentinite and listvenite is surrounded by rims of ferritchromite. During the formation of ferritchromite, Fe and to a lesser extent Mn are introduced into Cr-spinel, while Al, Mg and Cr diffuse outward. Hence ferritchromite rims have higher Cr/(Cr + Al) and lower $\text{Mg}/(\text{Mg} + \text{Fe}^{2+})$ than unaltered cores. The marked depletion of MnO in ferritchromite in carbonate listvenite can be attributed to the



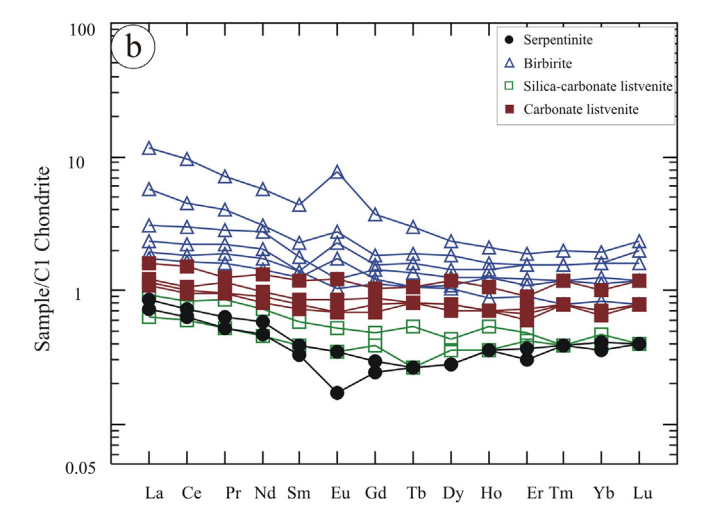


Fig. 10. (a) Primitive mantle-normalized trace element patterns for the averages of the Ess serpentinite and listvenites. Normalization values from McDonough and Sun (1995). **(b)** Chondrite-normalized rare earth element patterns of the Ess listvenites and serpentinite. Chondrite normalization values are from Evensen et al. (1978).

presence of carbonate minerals, a favorable sink for Mn (Deer et al., 1992). The absence of Cr-magnetite around the ferritchromite zone of Cr-spinel in the carbonate listvenite indicates that the ferritchromite was prevented from re-equilibrating with surrounding silicates due to the large modal abundance of carbonates.

The presence of kämmererite in the Ess serpentinites reflects replacement of Cr-spinel during later alteration or regional metamorphism. The significant Cr content of kämmererite and its petrographic relationship to primary relics of Cr-spinel suggest that this type of chlorite forms after primary Cr-spinel, perhaps during its alteration to ferritchromite. As noted above, excess Al, Cr and Mg are liberated from spinel during alteration to ferritchromite; these react with serpentine minerals to produce kämmererite (Azer and Stern, 2007).

7.3. Protolith and geodynamic setting of serpentinites

Relict textures and geochemical data indicate a highly depleted mantle protolith for the Ess serpentinite. Petrographic examination reveals abundant mesh and bastite texture, which are diagnostic of serpentine after olivine and orthopyroxene, respectively. The variable relative proportions of mesh and bastite indicate a range from harzburgite to dunite protoliths. Furthermore, the low MgO/SiO₂ ratios (<1.1) and TiO₂ contents (<0.02 wt%) of the serpentinite samples are

typical of supra-subduction zone depleted peridotites (e.g. Deschamps et al., 2013; Salters and Stracke, 2004). More specifically, the very low CaO (0.3–1.2 wt%) and Al $_2$ O $_3$ (0.5–0.8 wt%) contents resemble typical fore-arc peridotites (e.g. Ishii et al., 1992) and the very low Al $_2$ O $_3$ /SiO $_2$ ratios (<0.02) also suggest a fore-arc setting in which the protoliths of the serpentinites experienced high degrees of partial melting.

Cr-spinel has been used successfully as a geotectonic and petrogenetic indicator mineral, because its composition is notably sensitive to changes in temperature, pressure, oxygen fugacity, bulk rock and fluid composition (e.g. Arif and Jan, 2006; Azer et al., 2019; Barnes and Röeder, 2001; Dick and Bullen, 1984; Gahlan et al., 2020a; Gahlan et al., 2020b; Gamal El Dien et al., 2019; Jan and Windley, 1990). It is evident that Cr-spinel resists the low-temperature alteration processes that affect every other phase in an ultramafic sample. In the case of the Ess serpentinite, the high Cr# (>0.60) and low TiO₂ content (< 0.2 wt%) of relict primary Cr-spinel, and the high Fo content of coexisting olivine (Fo₉₁₋₉₃) argue for a depleted mantle protolith that suffered extensive partial melting in a supra-subduction zone setting, most likely in the fore-arc (e.g. Bloomer et al., 1995; Dick and Bullen, 1984; Ishii et al., 1992; Proenza et al., 2004). The high Cr# of fresh chromian spinels in Ess serpentinite requires either high degrees of partial melting extraction or extensive melt-rock interaction (e.g. Gamal El Dien et al., 2019; Matsukage and Kubo, 2003; Okamura et al., 2006; Parkinson and Pearce, 1998; Pearce et al., 2000). However, the low TiO₂ contents of the spinels are not consistent with the products of melt-rock reaction, which tend to be Ti-rich. On the Cr# versus Mg# discrimination diagram, fresh Cr-spinel relics from serpentinites and different types of listvenite plot in the region of fore-arc peridotite

Degrees of partial melting, estimated based on the Cr# of fresh spinel cores, are 33 to 39 wt% (Fig. 12), similar to those of supra-subduction zone peridotites (15–40 wt%; Parkinson and Pearce, 1998; Pearce et al., 2000). Such large degrees of partial melting, exceeding the exhaustion of clinopyroxene from the residue, are consistent with formation in a fore-arc setting (e.g., Gamal El Dien et al., 2019; Pearce et al., 2000). In this regard, the Ess ophiolite share a common tectonic setting with most Arabian Shield ophiolites, fragments of oceanic lithosphere emplaced above a subduction zone in a fore-arc setting (e.g. Abuamarah et al., 2020; Gahlan et al., 2020a; Gahlan et al., 2020b).

7.4. Petrogenesis of the listvenites

Listvenite is a product of hydrothermal alteration of ultramafic rocks, a process whereby primary silicate minerals are replaced by an assemblage of carbonates, quartz, and chromian micas (Buisson and Leblanc, 1987; Halls and Zhao, 1995; Plissart et al., 2009). During extensive carbonatization and silicification, the primary textures of the ultramafic silicate minerals are mostly obliterated; however, the presence of relict Cr-spinel and some patches of antigorite confirm that listvenite forms by replacement of an ultramafic protolith. Chemically, the elevated whole-rock Cr, Co and Ni contents are inherited from ultramafic precursors.

The ultimate sources of the hydrothermal fluids that drive listvenitization remain unclear. Systematic stable isotope (C, O, H) studies are generally considered necessary for distinguishing the temperature of alteration, and the composition and source of metasomatic agents (e.g. Bjerga et al., 2015; Boskabadi et al., 2017; Mirnejad et al., 2008; Zedef et al., 2000). Yet after a number of stable isotope studies, listvenites in various localities have been variously attributed to (1) mantle-derived CO₂-bearing fluids during near-ridge oceanic crust formation (e.g. Boskabadi et al., 2017; Colvine et al., 1984; Hamdy and Gamal El Dien, 2017; Stern and Gwinn, 1990), (2) meteoric and metamorphic hydrothermal fluids penetrating along tectonic fractures during or even after exhumation to upper crustal levels (e.g. Auclair et al., 1993; Buisson and Leblanc, 1987; Hamdy and Lebda, 2007; Likhoidov et al., 2007), and (3) mixing of these two sources (Gahlan et al., 2018).

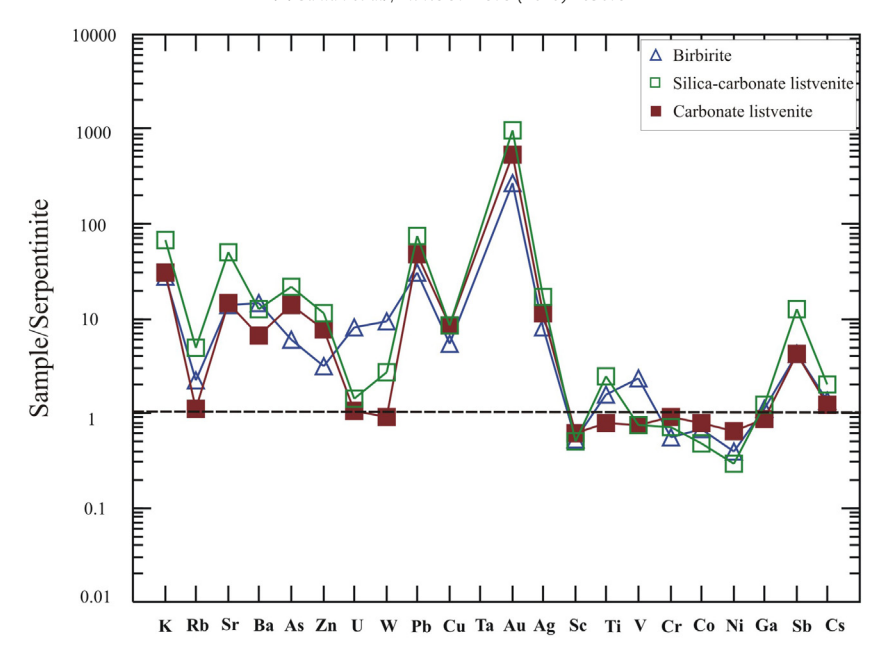


Fig. 11. Average trace element abundances in each type of listvenite, normalized to the average of the associated serpentinite, in order to emphasize changes in bulk chemistry during metasomatism.

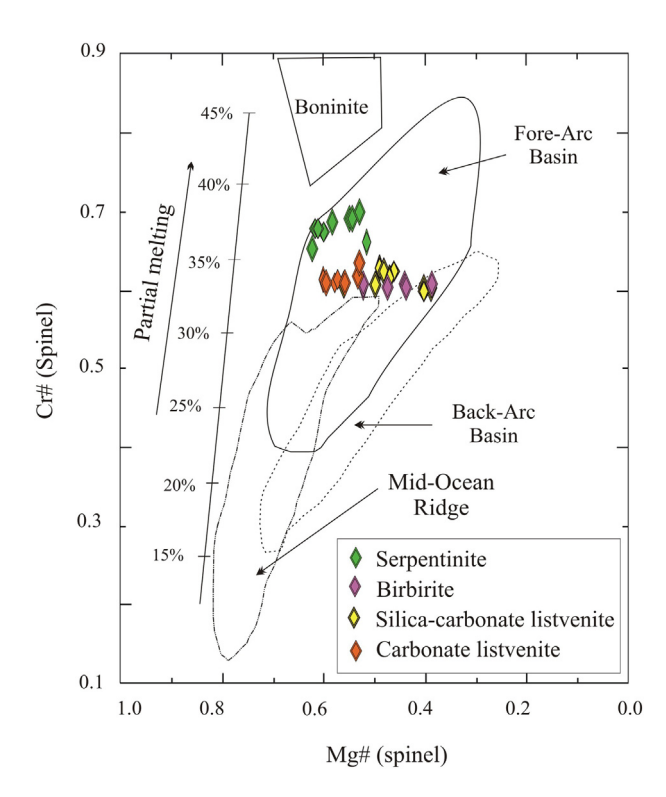


Fig. 12. Cr# vs. Mg# diagram for fresh relics of chromian spinel in the Ess ophiolitic serpentinite and listvenites. The field boundaries are from Dick and Bullen (1984), Bloomer et al. (1995), and Ohara et al. (2002).

We do not have stable isotope data on the Jabal Ess suite at this time, but we note that such data remain subject to a variety of interpretations and may not be sufficient to settle the issue of fluid sources.

Based on field and textural observations, it is very likely that listvenitization affected the Ess serpentinite in three successive stages, yielding the three distinct types of listvenite. High-temperature deformation fabrics and schistosity in the carbonate listvenite imply that

initial listvenitization took place at temperatures similar to those where serpentinization of primary ultramafic precursors takes place. On the other hand, the absence of deformation fabrics in the silica-carbonate listvenite and birbirite suggests that they postdate serpentinization.

If the first stage of listvenitization was contemporaneous with serpentinization, then it likely dates to the initial emplacement of the mantle section of the Ess ophiolite into fore-arc oceanic lithosphere near a spreading center. The source of CO₂ at this stage was probably decomposition of subducted, carbonate-bearing sedimentary rocks delivered to the underlying accretionary prism by oceanic subduction (Azer et al., 2019). Fluids carrying this CO₂ infiltrated upwards through the deforming and serpentinizing fore-arc upper-plate lithosphere, developing carbonate listvenite along fractures.

The second stage of listvenitization formed silica-carbonate listvenite from serpentinite or from carbonate listvenite along shear zones during ophiolite obduction. Silica-carbonate listvenite is inevitably found in the hanging walls of thrust sheets; hence the basal thrust that accommodated ophiolite obduction may have been the main conduit for fluid influx. The most likely source of SiO₂- and CO₂-bearing fluids at this stage is the footwall of the obduction thrust structure. Continental shelf sequences are likely to contain abundant pore fluid that is both silica- and carbonate-saturated. The migration of SiO₂- and CO₂bearing hydrothermal fluids through serpentinites can form quartzcarbonate assemblages through serpentine-consuming reactions (Halls and Zhao, 1995) such as $Mg_3Si_2O_5(OH)_4 + 3CO_2 \Rightarrow 3MgCO_3 +$ $2SiO_2 + 2H_2O$. Although this balanced reaction indicates that serpentine decomposition is the source of silica, it is necessary in general that the fluids remain silica-saturated or quartz will not precipitate; the existence of carbonate listvenite without quartz shows that this is not always the case. A flux of fluids already rich in dissolved silica seems necessary to instead form silica-carbonate listvenite. Fluids introduced at this stage were highly oxidizing and contributed to oxidation of relict Cr-spinel to form ferritchromite and Cr-magnetite in both serpentinites and silica-carbonate listvenite. Note that serpentinization of fresh peridotite at seafloor temperatures may produce magnetite under reducing conditions while evolving molecular hydrogen, e.g. at the Lost City hydrothermal field. However, production of magnetite during de-serpentinization requires an external oxidant.

The material that we have classified as birbirite at the Jabal Ess has previously been described by some authors as "hydrothermal chert lenses" (Al-Shanti, 1982; Johnson et al., 2004). Our field observations indicate that birbirite formed at the expense of other listvenites; the main observation driving this conclusion is the presence of carbonate-bearing listvenite fragments within birbirite. We also note the close affinity between the levels of gold enrichment in birbirite and in the other listvenite varieties, and the obvious contrast with the gold concentrations in serpentinite. We presume that late hydrothermal fluids passing along weak areas and fault planes at this stage were saturated in silica but low in dissolved carbonate. The birbirite samples are generally enriched in REE contents compared to the other listvenites; this reflects REE input the fluid phase, as it would be difficult to generate the observed level or pattern of enrichment simply by removing other components from the mass of the rock during metasomatism (Bau, 1991; Gillis et al., 1992; Tsikouras et al., 2006). The distinction between Fe₂O₃-rich and Fe₂O₃-poor birbirite most likely indicates that some birbirite formed directly from Fe-bearing serpentinite, whereas in other cases it formed from earlier, carbonate-bearing listvenite from which Fe had already been leached.

7.5. Chlorite geothermometer

Kranidiotis and MacLean (1987) provide a calibrated geothermometry equation for chlorite formation. The temperatures calculated with the equation for analyzed chlorite in listvenite and serpentinite are listed in Supplementary Table S5. Chlorite in serpentinite records the highest temperatures (266-330 °C; av. 292 °C). There appears to be a consistent decrease in chlorite formation temperature through the varieties of listvenite samples in the petrogenetic sequence we have inferred, with the highest recorded temperatures in carbonate listvenite (242-260 °C, av. 253 °C), intermediate values in silicacarbonate listvenite (223-241 °C, av. 234 °C), and the lowest temperatures in birbirite (200-219 °C, av. 208 °C). Given the uncertainty in the chlorite analyses and in the calibration of the geothermometer, the consistency observed is remarkable. The estimated chlorite temperatures from our study are nearly similar to the temperatures for listvenite formation proposed by Wilde et al. (2002) and many other authors for examples worldwide (e.g., Buisson and Leblanc, 1987; Oskierski et al., 2013; Schandl and Gorton, 2012). However, slightly higher temperatures have been suggested for listvenites in the Eastern Desert of Egypt (Gahlan et al., 2018).

8. Summary

- Listvenite is found in the mantle section of the Ess ophiolite, generally in the hanging walls of a series of imbricate thrust faults, with serpentinized ultramafic rocks in footwalls. Geochemical and textural evidence notably the presence of Cr-spinel relics and occasional patches of serpentine shows that, despite extensive metasomatism and mineral replacement, listvenite forms by replacement of ultramafic precursors.
- Listvenite samples in the study area range in color from grey to brown. They contain variable amounts of carbonates and quartz with disseminated fuchsite, sulfides, talc, chlorite, magnetite and chromite. Mineralogically, the listvenites are distinguished into three types: carbonate, silica-carbonate and silica listvenite (birbirite).
- Carbonate and silica-carbonate listvenites are found as relict fragments within birbirite and are replaced by birbirite along fractures and foliation planes, indicating that birbirite is the youngest of these alteration products.
- 4. The mantle section of the Jabal Ess experienced three successive stages of fluid alteration, recorded by the three types of listvenites. Based on deformation textures, the first stage was apparently contemporaneous with serpentinization and emplacement of the

- ophiolite into oceanic lithosphere. The second stage formed the silica-carbonate listvenite; it accompanied collisional tectonics and ophiolite obduction. Birbirite formed in the final stage, by silicification of both serpentinite and earlier listvenites. The first stage was associated with infiltration of CO_2 -bearing fluids likely released from the slab underlying the original fore-arc spreading center, whereas SiO_2 -saturated and CO_2 -bearing fluids driving the second stage were likely derived from the footwall of the thrust structure that accommodated ophiolite obduction onto a continental shelf.
- 5. Cr-spinel relics in both serpentinite and listvenite have high Cr#, typical of spinel in residual peridotites associated with supra-subduction zone environments, and more specifically with fore-arc settings. A minor redistribution of Cr and Al during listvenitization is indicated by a modestly lower Cr# of spinel cores in all listvenites, compared to their serpentinite protoliths. However, relict Cr-spinel in serpentinite and in carbonate listvenite have significantly higher Mg# than that in silica-carbonate and in birbirite, suggesting low-temperature re-equilibration of Fe and Mg between Cr-spinel and silicates in silica-bearing listvenites.
- 6. The sequence of alteration processes recorded by the ultramafic section of the Ess ophiolite includes serpentinization and three distinct episodes of listvenitization. However, all the listvenites are highly enriched in gold relative to the serpentinites. Either the first, carbonate-forming stage, accomplished the bulk of gold concentration which was then inherited by subsequent listvenite varieties or all three stages of listvenitization induced similar levels (1 to 3 orders of magnitude) of enrichment in precious metals, especially gold. Gold grades up to 3000 ng/g in listvenite suggest that Jabal Ess is a plausible prospect for economic gold recovery.
- 7. The temperatures obtained for chlorite formation in listvenite and serpentinite indicate a systematic cooling sequence from serpentinite through carbonate listvenite, silica-carbonate listvenite, and birbirite.

Declaration of Competing Interest

The authors declare that they have no known competing financial interests or personal relationships that could have appeared to influence the work reported in this paper.

Acknowledgements

Special thanks are paid to King Saud University, Deanship of Scientific Research, Research Group No. RG-1436-036, for their support. PDA acknowledges support from the US NSF, award EAR-1947616. The authors are also indebted to the editor (Prof. Michael Roden) and two anonymous reviewers for their efforts and numerous helpful comments.

Appendix A. Supplementary data

Supplementary data to this article can be found online at https://doi.org/10.1016/j.lithos.2020.105679.

References

- Abuamarah, B.A., Asimow, P.D., Azer, M.K., Ghrefat, H., 2020. Suprasubduction-zone origin of the podiform chromitites of the Bir Tuluhah ophiolite, Saudi Arabia, during Neoproterozoic assembly of the Arabian Shield. Lithos 360–361, 105439.
- Al Jahdali, N.S., 2004. Geology of Jabal Ghadarah Area, Bir Tawilah District with Special Emphasis on Listvenite as a Potential Source for Gold in the Kingdom of Saudi Arabia. M.Sc Thesis. King AbdulAziz University, Jeddah, KSA, p. 197.
- Al Jahdali, N.S., Harbi, H., Eldougdoug, A., 2003. Gold bearing listvenite in Jabal Al Ghadarah area, Central Arabian Sheild, Kingdom of Saudi Arabia. Proceedings of the 8th Arab Conference on Mineral Resources, Sanaá. Republic of Yemen, 13-16 October, 1, pp. 26–43.
- Al Shanti, A.M.S., 2009. Geology of the Arabian Shield of Saudi Arabia. Scientific Publications Centre, King Abdulaziz University, Jeddah, KSA.

- Ali, K.A., Azer, M.K., Gahlan, H.A., Wilde, S.A., Samuel, M.D., Stern, R.J., 2010. Age of formation and emplacement of Neoproterozoic ophiolites and related rocks along the Allaqi Suture, south Eastern Desert, Egypt. Gondw. Res. 18, 583–595.
- Al-Shanti, M.M.S., 1982. Geology and Mineralization of the Ash Shizm-Jabal Ess Area (Doctoral Dissertation, Ph. D. thesis). King Abdulaziz University, Jiddah, p. 291.
- Arif, M., Jan, M.Q., 2006. Petrotectonic significance of the chemistry of chromite in the ultramafic-mafic complexes of Pakistan. J. Asian Earth Sci. 27, 628–646.
- Auclair, M., Gauthier, M., Trottier, J., Jebrak, M., Chartrand, F., 1993. Mineralogy, geochemistry, and paragenesis of the Eastern Metals serpentinite-associated Ni-Cu-Zn deposit, Quebec Appalachians. Econ. Geol. 88 (1), 123–138.
- Azer, M.K., 2013. Evolution and economic significance of listwaenites associated with Neoproterozoic ophiolites in south Eastern Desert, Egypt. Geol. Acta 11 (1), 113–128.
- Azer, M.K., Stern, R.J., 2007. Neoproterozoic (835–720 Ma) serpentinites in the Eastern Desert, Egypt: Fragments of fore-arc mantle. J. Geol. 115, 457–472.
- Azer, M.K., Gahlan, H.A., Asimow, P.D., Mubarak, H.S., Al-Kahtany, K.M., 2019. Multiple stages of carbonation and element redistribution during formation of ultramafichosted magnesite in Neoproterozoic ophiolites of the Arabian-Nubian Shield, Egypt. J. Geol. 127 (1), 81–107.
- Barnes, S.J., Röeder, P.L., 2001. The range of spinel compositions in terrestrial mafic and ultramafic rocks. J. Petrol. 42, 2279–2302.
- Bau, M., 1991. Rare-earth element mobility during hydrothermal and metamorphic fluid-rock interaction and the significance of the oxidation state of europium. Chem. Geol. 93 (3–4), 219–230.
- Beinlich, A., Plümper, O., Hövelmann, J., Austrheim, H., Jamtveit, B., 2012. Massive serpentinite carbonation at Linnajavri, N–Norway. Terra Nova 24 (6), 446–455.
- Belogub, E.V., Melekestseva, I.Y., Novoselov, K.A., Zabotina, M.V., Tret'yakov, G.A., Zaykov, V.V., Yuminov, A.M., 2017. Listvenite-related gold deposits of the South Urals (Russia): A review. Ore Geol. Rev. 85, 247–270.
- Bjerga, A., Konopásek, J., Pedersen, R.B., 2015. Talc-carbonate alteration of ultramafic rocks within the Leka Ophiolite Complex, Central Norway. Lithos 227, 21–36.
- Bloomer, S.H., Taylor, B., MacLeod, C.J., Stern, R.J., Fryer, P., Hawkins, J.W., Johnson, L., 1995. Early arc volcanism and ophiolite problem: A perspective from drilling in the Western Pacific. In: Taylor, B., Natland, J. (Eds.), Active Margins and Marginal Basins of the Western Pacific, Geophysical Monograph. American Geophysical Union vol. 88. Washington, DC, pp. 1–30.
- Bonatti, E., Michael, P.J., 1989. Mantle peridotites from continental rifts to oceanic basins to subduction zones. Earth Planet. Sci. Lett. 91, 297–311.
- Boskabadi, A., Pitcairn, I.K., Broman, C., Boyce, A., Teagle, D.A.H., Cooper, M.J., Azer, M.K., Mohamed, F.H., Stern, R.J., Majka, J., 2017. Carbonate alteration of ophiolitic rocks in the Arabian–Nubian Shield of Egypt: sources and compositions of the carbonating fluid and implications for the formation of Au deposits. Int. Geol. Rev. 59 (4), 391–419.
- Botros, N.S., 2002. Metallogeny of gold in relation to the evolution of the Nubian Shield in Egypt. Ore Geol. Rev. 19, 137–164.
- Boyle, R.W., 1979. The geochemistry of gold and its deposits. Geol. Survey Canada Bull. 280, 333–361.
- Buckman, S., Ashley, P.M., 2010. Silica-carbonate (listwanites) related gold mineralization associated with epithermal alteration of serpentinite bodies. Manager 2010 (May 2014). 94–105.
- Buisson, G., Leblanc, M., 1987. Gold in mantle peridotites from Upper Proterozoic ophiolites in Arabia, Mali, and Morocco. Econ. Geol. 82 (8), 2091–2097.
- Coish, R.A., Gardner, P., 2004. Suprasubduction-zone peridotite in the northern USA Appalachians: evidence from mineral composition. Mineral. Mag. 68, 699–708.
- Colvine, A.C., Andrews, A.J., Cherry, M.E., Durocher, M.E., Fyon, A.J., Lavigne, M.J., Macdonald, A.J., Marmont, S., Poulsen, K.H., Springer, J.S., Troop, D.G., 1984. An integrated model for the origin of Archean lode gold deposits. Ontario Geological Survey. Open File Report 5524, 98.
- Deer, W.A., Howie, R.A., Zussman, J., 1992. An Introduction to the Rock Forming Minerals. Second edition. Longman Scientific and Technical, London, p. 696.
- Deschamps, F., Godard, M., Guillot, S., Hattori, K., 2013. Geochemistry of subduction zone serpentinites: a review. Lithos 178, 96–127.
- Dick, H.J., Bullen, T., 1984. Chromian spinel as a petrogenetic indicator in abyssal and alpine-type peridotites and spatially associated lavas. Contrib. Mineral. Petrol. 86 (1), 54–76.
- Evensen, N.M., Hamilton, P.J., O' Nions, R.K., 1978. Rare earth abundances in chondritic meteorites. Geochim. Cosmochim. Acta 42 (8), 1199–1212.
- Gahlan, H.A., Azer, M.K., Asimow, P.D., Mubarak, H.S., Al-Kahtany, K.M., 2020a. Petrological characteristics of the Neoproterozoic Ess ophiolite mantle section, Arabian Shield, Saudi Arabia: a mineral chemistry perspective. Int. J. Earth Sci. 109, 239–251.
- Gahlan, H.A., Azer, M.K., Asimow, P.D, Al-Kahtany, K.M., 2020b. Genesis and geodynamic evolution of serpentinized ultramafics and the associated magnesite deposits, Al-Wask ophiolite, Arabian Shield, Saudi Arabia. Am. J. Sci. 320, 236–279.
- Gamal El Dien, H., Arai, S., Doucet, L.-S., Li, Z.-X., Kil, Y., Fougerouse, D., Reddy, S.M., Saxey, D.W., Hamdy, M., 2019. Cr-spinel records metasomatism not petrogenesis of mantle rocks. Nat. Commun. 10, 1–12.
- Gillis, K.M., Ludden, J.N., J.N., Smith, A.D. 1992. Mobilization of the REE during crustal aging in the Troodos ophiolite, Cyprus. Chem. Geol. 98, 71–86.
- Halls, C., Zhao, R., 1995. Listvenite and related rocks: perspectives on terminology and mineralogy with reference to an occurrence at Cregganbaun, Co. Mayo, Republic of Ireland. Miner. Deposita 30 (3–4), 303–313.
- Hamdy, M.M., Gamal El Dien, H.M., 2017. Nature of serpentinization and carbonation of ophiolitic peridotites (Eastern Desert, Egypt): constrains from stable isotopes and whole rock geochemistry. Arab. J. Geosci. 10 (19), 429.
- Hamdy, M.M., Lebda, E.M., 2007. Metamorphism of ultramafic rocks at Gebel Arais and Gebel Malo Grim, Eastern Desert, Egypt: mineralogical and O-H stable isotopic constraints. Egypt. J. Geol. 51, 105–124.

- Hansen, L.D., Dipple, G.M., Gordon, T.M., Kellett, D.A., 2005. Carbonated serpentinite (listvenite) at Atlin, British Columbia: a geological analogue to carbon dioxide sequestration. Can. Mineral. 43 (10), 225–239.
- Harbi, H.M., Hassanen, M.A., Eldougdoug, A.A., Sahal, M.S.A., 2003. Geological and geochemical studies on some gold occurrences in Zalim Quadrangle, Western Afif terrane, Arabian shield, Kingdom of Saudi Arabia. King Abdul Aziz University Research Council, Project No. 421/203, 69p.
- Harbi, H., Eldougdoug, A., Al Jahdali, N.S., 2006. Geology and Geochemistry of Jabal Ghadarah Ophiolitic mélange, Zalim Quadrangle, Central Saudi Arabia. J. King Abdulaziz Univ. (Earth Sciences) 17, 117–153.
- Hey, M.H., 1954. A new review of the chlorites. Mineral. Mag. 30, 272-292.
- Hinsken, T., Brocker, M., Strauss, H., Bulle, F., 2017. Geochemical, isotopic and geochronological characterization of listvenite from the Upper Unit on Tinos, Cyclades, Greece. Lithos 282–283, 281–297.
- Ishii, T., Robinson, P.T., Maekawa, H., Fiske, R., 1992. Petrological studies of peridotites from diapiric Serpentinite Seamounts in the Izu- Ogasawara-Mariana forearc, leg 125. In: Pearce, J., Stokking, L.B., et al. (Eds.), Proceedings of the Ocean Drilling Project, Leg 125, Scientific Results (College Station), pp. 455–485.
- Ishimaru, S., Ishida, Y., Shirasaka, M., Okrugin, V.M., 2007. Melting and multi-stage metasomatism in the mantle wedge beneath a frontal arc inferred from highly depleted peridotite xenoliths from the Avacha Volcano, Southern Kamchatka. J. Petrol. 48, 395–433.
- Jan, M.Q., Windley, B.F., 1990. Chromian spinel–silicate chemistry in ultramafic rocks of the Jijal complex, Northwest Pakistan. J. Petrol. 31, 667–715.
- Johnson, P.R., Woldehaimanot, B., 2003. Development of the Arabian-Nubian Shield: Perspectives on accretion and deformation in the northern East African Orogen and the assembly of Gondwana. In: Yoshida, M., Dasgupta, S., Windley, B. (Eds.), Proterozoic East Gondwana: Supercontinent assembly and breakup. 206. Geological Society of London Special Publications, pp. 289–325.
- Johnson, P.R., Kattan, F.H., Al-Saleh, A.M., 2004. Neoproterozoic ophiolites in the Arabian Shield: Field relations and structure. Develop. Precambrian Geol. 13, 129–162.
- Kranidiotis, P., MacLean, W.H., 1987. The systematics of chlorite alteration at the Phelps Dodge massive sulfide deposit, Matagami, Quebec. Econ. Geol. 82, 1898–1911.
- Leake, B.E., Woolley, A.R., Arps, C.E.S., Birch, W.D., Gilbert, M.C., Grice, J.D., Hawthorne, F.C., Kato, A., Kisch, H.J., Krivovichev, V.G., Linthout, K., Laird, J., Mandarino, J., Maresch, W.V., Nickel, E.H., Rock, N.M.S., Schumacher, J.C., Smith, D.C., Stephenson, N.C.N., Ungaretti, L., Whittaker, E.J.W., Youzhi, V., 1997. Nomenclature of amphiboles: Report of the Subcommittee on Amphiboles of the International Mineralogical Association Commission on New Minerals and Mineral Names. Mineral. Mag. 61, 295–321.
- Likhoidov, G.G., Plyusnina, L.P., Shcheka, Z.A., 2007. The behavior of gold during listvenitization: Experimental and theoretical simulation. Doklady Earth Sci. 415 (5), 723–726, July.
- Matsukage, K.N., Kubo, K., 2003. Chromian spinel during melting experiments of dry peridotite (KLB-1) at 1.0–2.5 GPa. Am. Mineral. 88, 1271–1278.
- McDonough, W.F., Sun, S.S., 1995. Composition of the Earth: Chemical Geology. 120 pp. 223–253.
- Mirnejad, H., Ebrahimi-Nasrabadi, K., Lalonde, A.E., Taylor, B.E., 2008. Mineralogy, stable isotope geochemistry, and paragenesis of magnesite deposits from the ophiolite belt of Eastern Iran. Econ. Geol. 103, 1703–1713.
- Morimoto, N., Fabries, J., Ferguson, A., Ginzburg, I., Ross, M., Seifert, F., Zussman, J., Aoki, K., Gottardi, G., 1988. Nomenclature of pyroxenes. Mineralogical Magazine 52, 535–550.
- Nehlig, P., Genna, A., Asfirane, F., 2002. A review of the Pan-African evolution of the Arabian Shield. GeoArabia 7, 103–124.
- Ohara, Y., Stern, R.J., Ishii, T., Yurimoto, H., Yamazaki, T., 2002. Peridotites from the Mariana Trough: first look at the mantle beneath an active back-arc basin. Contrib. Mineral. Petrol. 143, 1–18.
- Okamura, H., Arai, S., Kim, Y.U., 2006. Petrology of Forearc Peridotite from the Hahajima Seamount, the Izu-Bonin Arc, with Special Reference to Chemical Characteristics of.
- Oskierski, H.C., Bailey, J.G., Kennedy, E.M., Jacobsen, G., Ashley, P.M., Dlugogorski, B.Z., 2013. Formation of weathering-derived magnesite deposits in the New England Orogen, New South Wales, Australia: implications from mineralogy, geochemistry and genesis of the Attunga magnesite deposit. Miner. Deposita 48, 525–541.
- Osman, A., 1995. The mode of occurrence of gold-bearing listvenite at El Barramiya gold mine, Eastern desert, Egypt. Middle East Research Centre. Ain Shams University. Earth Sciences Series 9, 93–103.
- Pallister, J.S., Stacey, J.S., Fischer, L.B., Premo, W.R., 1988. Precambrian ophiolites of Arabia: Geologic settings, U-BP geochronology, BP-isotope characteristics, and implications for continental accretion. Precambrian Res. 38, 1–54.
- Parkinson, I.J., Pearce, J.A., 1998. Peridotites from the Izu-Bonin-Mariana forearc (ODP Leg 125): evidence for mantle melting and melt-mantle interaction in a suprasubduction zone setting. J. Petrol. 39, 1577–1618.
- Pearce, J.A., Barker, P.F., Edwards, S.J., Parkinson, I.J., Leat, P.T., 2000. Geochemistry and tectonic significance of peridotites from the South Sandwich arc-basin system, South Atlantic. Contrib. Mineral. Petrol. 139, 36–53.
- Pirouei, M., Kolo, K., Kalaitzidis, S.P., 2020. Hydrothermal listvenitization and associated mineralizations in Zagros Ophiolites: Implications for mineral exploration in Iraqi Kurdistan. J. Geochem. Explor. 208, 106–404.
- Plissart, G., Féménias, O., Māruntiu, M., Diot, H., Demaiffe, D., 2009. Mineralogy and geothermometry of gabbro-derived listvenites in the Tisovita–Iuti ophiolite, Southwestern Romania. Can. Mineral. 47 (1), 81–105.
- Proenza, J.A., Ortega-Gutierrez, F., Camprubi, A., Tritlla, J., Elias-Herrera, M., Reyes-Salas, M., 2004. Paleozoic serpentinites enclosed chromitites from Tehuitzingo (Acatla'n Complex, southern Mexico): a petrological and mineralogical study. J. South Am. Earth Sci. 16. 649–666.

- Ramadan, T.M., Sadek, M.F., Abu El Leil, I., Salem, S.M., 2005. Um El Touyur El Fuqani gold mineralization, South Eastern Desert, Egypt: using Landsat ETM+ imagery. Ann. Geol. Survey Egypt 28, 263–281.
- Salters, V.J., Stracke, A., 2004. Composition of the depleted mantle. Geochem. Geophys. Geosyst. 5 (5).
- Schandl, E.S., Gorton, M.P., 2012. Hydrothermal alteration and ${\rm CO_2}$ metasomatism (natural carbon sequestration) of komatiites in the South-Western Abitibi greenstone belt. Can. Mineral. 50, 129–146.
- Stern, R.J., Gwinn, C.J., 1990. Origin of late Precambrian Intrusive Carbonates, Eastern Desert of Egypt and Sudan: C, O, and Sr Isotopic evidence. Precambrian Res. 46, 259–272.
- Stern, R.J., Johnson, P.R., Kröner, A., Yibas, B., 2004. Neoproterozoic ophiolites of the Arabian-Nubian Shield. In: Kusky, T.M. (Ed.), Precambrian Ophiolites and Related Rocks. Developments in Precambrian Geology vol. 13. Elsevier, Amsterdam, pp. 95–128.
- Stoeser, D.B., Frost, C.D., 2006. Nd, Pb, Sr and O isotopic characterization of Saudi Arabian Shield terranes. Chem. Geol. 226, 163–188.
- Tsikouras, B., Karipi, S., Grammatikopoulos, T.A., Hatzipanagiotou, K., 2006. Listwaenite evolution in the ophiolite melange of Iti Mountain (continental Central Greece). Eur. J. Mineral. 18 (2), 243–255.

- Uçurum, A., 2000. Listwaenites in Turkey: perspectives on formation and precious metal concentration with reference to occurrences in east-Central Anatolia. Ofioliti 25 (1), 15–29
- Uçurum, A., Larson, L.T., 1999. Geology, Base-precious Metal Concentration and Genesis of the Silica-Carbonate Alteration (Listvenites) from Late Cretaceous Ophiolitic Mélanges at Central East Turkey. Chem. Erde-Geochem. 59 (2), 77–104.
- Uysal, I., Ersoy, E.Y., Dilek, Y., Kapsiotis, A., Sarıfakıoğlu, E., 2016. Multiple episodes of partial melting, depletion, metasomatism and enrichment processes recorded in the heterogeneous upper mantle sequence of the Neotethyan Eldivan ophiolite, Turkey. Lithos 246, 228–245.
- Van Noort, R., Spiers, C.J., Drury, M.R., Kandianis, M.T., 2013. Peridotite dissolution and carbonation rates at fracture surfaces under conditions relevant for in situ mineralization of CO₂. Geochim. Cosmochim. Acta 106, 1–24.
- Wilde, A.R., Simpson, L., Hanna, S., 2002. Preliminary Study of tertiary hydrothermal alteration and platinum deposition in the Oman ophiolite. J. Virtual Explorer 6, 7–19. Zedef, V., Russell, M.J., Fallick, A.E., Hall, A.J., 2000. Genesis of vein stockwork and sedi-
- Zedef, V., Russell, M.J., Fallick, A.E., Hall, A.J., 2000. Genesis of vein stockwork and sedimentary magnesite and hydromagnesite deposits in the ultramafic terrains of southwestern Turkey: a stable isotope study. Econ. Geol. 95, 429–446.
- Zoheir, B.A., Lehmann, B., 2011. Listvenite-lode association at the Barramiya gold mine, Eastern Desert, Egypt. Ore Geol. Rev. 39, 101–115.